Termites: The Marvelous Cladder and Thermoregulator in Nature: New Discoveries

Sherif Shawki Hindi *, Shatha A. Alqurashi *, Naimah Asid Alanazi , Khalid. A. Asiry

Posted Date: 22 September 2023

doi: 10.20944/preprints202309.1492.v1

Keywords: termite; thermoregulator; nest mortar; lignin; microcrystalline cellulose; nanocrystalline cellulose

Article

Termites: The Marvelous Cladder and Thermoregulator in Nature: New Discoveries

Sherif S. Hindi [1,*], Shatha Alqurashi [2], Naimah Asid Alanazi [3] and Khalid A. Asiry [1]

[1] Department of Agriculture, Faculty of Environmental Sciences, King Abdullaziz University (KAU), Jeddah 21589, Saudi Arabia; Kasiry@kau.edu.sa_

[2] Department of Biology, College of Science, University of Jeddah, Jeddah, Saudi Arabia; saaqurshi@uj.edu.sa

[3] Department of Biology, Faculty of Science, University of Ha'il, P.O. Box 659, Ha'il 81421, Saudi Arabia; N.alenezy@uoh.edu.sa

Abstract: The mortar's composition, porosity, mechanical properties, entryways' orientation, and conditioning status of the tunnels made by the Najdian Termite, *Microtermes najdensis* located at Hada Al-Sham village, Makkah Province, Saudi Arabia were studied. The most prevalent infected timber trees by this pest were *Tamarix aphylla*, *Pithecellobium duce*, *Zizyphus spina christi*, *Leucaena leucocephala*, *Ficus infectoria*, and *Phoenix dactylifera*. Climate, soil, healthy wood (Wh), and termite nest skeleton (TNS) were the four components of the termite system that were investigated physically, chemically, spectroscopically, and by FTIR, XRD, SEM, and TEM. It was noticed that the entryways of the termite nests are located at the southwest direction for all the infected trees studied at Hada Al-Sham village that promotes better ventilation. Concerning to the air-conditioning status within the their nest, the internal temperature (IT) was found to be milder than that for its analogous value for the outer temperature (OT) in which the IT was wormer than OT during cold durations, while it was colder than the hottest OT in hot days and vice versa. The IT's trend had more constantancy with minor fluctuations compared to that for the OT. Moreover, the IT was found to be tended to the upper OT's limit otherwise its colder one. This finding means that these termite species prefer the hotter atmospheres comparing the colder circumstances. Lignin is the prominent tracer of the organic matter used as a binder for the TNS due to its gluing ability, resistance to enzymatic degradation by the termites and their accompanied fungal community habituating the nests. The presence of both microcrystalline cellulose (MCC) and nanocrystalline cellulose (NCC) was discovered for the first time in the nest mortar reinforcing Klason lignin as the main binder. Their presence was proved by FTIR, XRD, SEM and TEM analyses and we satisfied that they were naturally-synthesized by the action of enzymatic hydrolysis excreted by the termites and their accompanied fungal community habituating the nests. The gross heat of combustion (GHCs) of the W_h and TNS were studied to try to find an important utilization of the infected woods as renewable energy resources instead of disposal them without economic benefits. These findings may be used for interpreting the durability of the termite nests to the different environmental stresses. Biomimicry of the termites' nest from the perspective of its magic mortar with a suitable permeability, the entryways' orientation, and the air-conditioning status can lead to modify the current construction's designs to be more green and ecofriendly.

Keywords: termite; thermoregulator; nest mortar; lignin; microcrystalline cellulose; nanocrystalline cellulose

Introduction

Many genera and species of termites have been brought from other countries inside shipments of wood and lumber, making them endemic permanent inhabitants [1]. According on its genealogy, termite colonies live in enclosed nests that are either subterranean (underground nests), arboreal (nests associated with trees), or epigeal (soil mounds) as referred by Li and Greening [2]. The effect

of three main ecological factors; vegetation, rainfall and landform on the distribution and abundance of five termite genera commonly found in Saudi Arabia has been studied. Five genera include Anacanthotermes, Psammotermes, Microcerotermes, Amitermes and microtermes. With the exception of termites of the genus Microtermes, those of the remaining 4 genera seem to have almost similar requirements. They prefer open scrubs (regions containing herbs and shrubs), moderate mean annual rainfall (ranging between 50 and 150ram), and are more abundant in plateau areas. On the contrary, Microtermes has 50 % of its sampling sites located in open scrubs and about 40 % in large trees/grass areas. It prefers relatively higher mean annual rainfall (ranging between 250 and 500 mm), and are more abundant in plains [3,4].

Numerous termite species, both native (endemic) and some introduced cosmopolitan species, are found in rural, urban, and suburban habitats [5]. The subterranean termites were classified ecologically into four groups, namely drywood termites, dampwood termites, and formosan termites [6,7]. *Microtermes najdensis*, a small underground termite of the Termitidae family, was discovered at Hada Al-Sham [7,8]. In addition, termites belonging to the Kaloter-mitidae, Hodotermitidae, Rhinotermitidae, and Termitidae families were discovered in Saudi Arabia at all. The first three of them are lesser termite families, whereas the fourth one is a high developed family termed as Termitidae [8]. The annual losses due to their heavy infestations in human life have reached a great level leading to apply prophylactic and preventive methods [8-12].

Nests provide a tight enclosure that protects the colony from predators including but not limited to ants, lizards and/or birds [13]. Termite nests are among the most diverse and complicated structures among the vast array of those constructed by animals [13]. Their intricate architectures and how termites use them have fascinated mankind for centuries, whether as part of local agricultural practice, a simple landscape feature, an inspiration for societal collective building, or a scientific study object on its own [13]. However, their nests are less well studied than those of many ants, social wasps, and social bees, particularly honey bees and stingless bees, because termites that create mounds or other prominent structures are of modest ecological relevance [13].

It was reported by Johst [13] and Turner and Soar [14] that termites' nest structures have been used as exemplars of bioinspired designs, in buildings, for air-conditioning control (adjusting internal temperature and relative humidity), balancing each of energy and gas- exchanging between inner and outer nest' system. Termite nests' constructions are often quite species-dependent meaning that different species in the same habitat can create nests of varying firmness. The chemical structure of their saliva and faecal material, as well as the clay/sand ratio, influence nest solidity [13].

Wood is constituted structurally from polysaccharides (cellulose and hemicelluloses) and lignin [15]. Cellulose has a homopolymeric structure which composed of [1→4]-β-D-glucopyranose monomers, understanding its conformation and the 3D-packing manner in microfibrils is still remains largely a mystery [16-18]. A cellulosic chain is made up of repeating cellobiose units, which provide a variety of structures, reactions, and uses, hence enhancing its significance [19]. Approximately 10.000 glucopyranose subunits (monomers) or more can be found in a single cellulose chain [20]. Hydrogen bonds along with Van der Waals forces help the neighboring chains stick together. Bio-hydrolyzing cellulose needs three cellulolytic enzymes at least to be synergized: endo-β-[1, 4]-glucanase which is able to hydrolyze β-1, 4-bonds of cellulose chains, exo-β-[1, 4]-cellobiohydrolase that librates cellobiose from the cellulose' s non-reducing ends, and β-glucosidase that hydrolyses cellobiose or longer chains releasing glucose monomers [21,22].

Beside cellulose, hemicelluloses are the second division of polysaccharides found in plant cell walls. It is made up of simple sugars' monomers, namely glucose, galactose, mannose, xylose, arabinose, and glucuronic acid. It has equatorial skeleton with β- [1→4]-linkages [15]. Hemicelluloses are found as different compounds spreading at all plants such as xylans, glucomannans, xyloglucans, mannans as well as beta-[1→3, 1→4]-glucans which are confined essentially to Poales [15]. Due to species and cell types, the structure of hemicellulose varies greatly in nature. Hemicelluloses' role in fortifying the cell wall is achieved by its interaction with other biopolymers. It was indicated that glycosyltransferases present at the Golgi membranes synthesize hemicelluloses [23]. In the primary walls of dicotyledons, xyloglucan predominates, and it significantly helps cellulosic microfibrils to

 doi:10.20944/preprints202309.1492.v1

be cross-linked together [24]. Moreover, pectins are a kind of heterogeneous polysaccharides that contain 1→4-linked α-D-galactosyluronic acid. From primary plant cell walls, homogalacturonan [HG], rhamnogalacturonan-I, and substituted galacturonans are three detected forms of pectin.

A phenolic polymer called lignin accounts for 15–36% of the biomass in wood. It performs a number of activities in plants' extracellular matrix [25]. It consists of phenylpropane monomers cross-linked by various chemical linkages is what gives lignin its complexity.

For the termite diets, it was reported that many xylophagous insects have symbiotic bacteria and/or protozoa in their digestive systems that help break down cellulose, but some of them, like the termite from the Termitidae family, have their own cellulose enzyme. Additionally, termites depend on a mutualistic gut microbiota to mediate the fermentation and hydrolysis of lignocellulose, which produces acetate, hydrogen (H_2), and methane as well as improves carbon and nitrogen cycles and modifies soil structures [2].

The main source of food for termites is wood, grass, leaves, humus, animal excrement from herbivores, and plant-based goods including paper, cardboard, and cotton. The numerous cellulosic-based foods from other dead or living plants are consumed by subterranean termites [2,26-28]. It makes sense that termites require three things to survive: food, water, and air. For nutrition, it was reported by Ulyshen [29] that some termites' groups depends on nutrition produced from decayed wood arisen by numerous developing fungi. The amazing and extraordinary behavior of these termites' species is their transferring fungus' spores by unique structures on their bodies called mycangia [29]. After that, they spread these spores within their nests' floor in order the spores will be able to continue their growth cycle. This process can be viewed as a farming practice [30,31].

For water needed for the termites within their nests, both dry wood- and damp wood-termites do not depend on the ground water but get water it from their food sources [dry wood] or from damp, dead, rotten wood, respectively [32]. Contrarily, subterranean termites are compelled to contact with soil to fulfill their thirst for water and moisture. As a result, subterranean termites have evolved into the most costly and damaging to human property, woodwork, stored goods, buildings, and wooden infrastructure [11].

It has been extensively recorded how termites forage or swarm to disperse in search of food or to build new nests and colonies. It is thought that some procedural swarming activity, which can occur indoors or outside, gives homeowners an early warning for early infestation by this insect [33-42].

Due to their stealthy eating habits, subterranean termites are nearly impossible to be detected unless their galleries, such as earth tubes and tunnels, are visible together with a significant infestation of wood that has been hollowed out and filled with fine earth particles [43-45].

The diet of termites is basically rich in cellulose and hemicelluloses as well as lignin or its derivatives. Termites digest lignocellulosic compounds due to the synergizing of their own enzymes and exogenous enzymes from microorganisms. Termites are divided into six feeding groups according to their diets, namely wood feeding, dry-wood feeding, wood and litter feeding, soil feeding, fungus growing and grass feeding termites. The termite gut promotes very specialized cellulolytic and hemicellulolytic microorganisms. The association between certain xylophagous termites and their hindgut protozoa is the fascinating nutritional symbiosis [21,46,47].

Hemicellulose has a random, amorphous structure with weak strength and is easily hydrolyzed by dilute reagents (acid, base, or numerous hemicellulase enzymes) in contrast to cellulose, which is crystalline, robust, and resistant to hydrolysis. Accordingly, hemicellulose is more easily broken down by termites than cellulose and is digested with high efficiency ranging from 49 to 78%. Hence the fundamental constituents of hemicellulose, known as xylans, are polysaccharides created from xylose units. Hemicellulose chain is broken down when beta-1, 4-xylan is broken down by the enzyme xylanase into xylose. Endo-1, 4-xylanase enzyme catalysis is required for the process. Termites can also have various carbohydrases, including sucrase, maltase, trehalase, and raffinase. Chitinase activity, which is made by microbial symbionts, was observed in *Neotermes bosei*. When there is a food shortage, cannibalism occurs [21,48].

 doi:10.20944/preprints202309.1492.v1

Lignin or its derivatives, cellulose, and hemicelluloses are abundant in the termites' diet. Termites may digest lignocellulosic materials thanks to the collaboration of their own enzymes and foreign enzymes from microbes. Termites can be divided into six feeding categories based on what they prefer to eat: wood, dry wood, wood and litter, soil, fungus, and grass. The termite stomach supports highly specialized cellulolytic and hemicellulolytic microbes. Certain xylophagous termites form an unusual nutritional relationship with their hindgut protozoa. Furthermore, termites and cockroaches' foreguts and midguts, as well as their salivary glands, showed cellulose activity, according to Slaytor [49]. These areas are the typical sites where digestive enzymes are secreted, and there are no or very few microorganisms present. Therefore, there is no proof that termite cellulose digestion is mediated by bacteria.

Lower and higher termites were reported to be differed in their abilities to digest cellulose. The lower termites produce many endogenous enzymes, including beta-glucosidases, exoglucanases, endoglucanases, chitinases which secreted particularly by their salivary glands as well as foregut. On the other hand, higher termites no longer consume healthy wood due to their deficient symbiotic bacteria in their gut, thus they favor partially fungal-decayed wood, or they raise fungi in elaborate gardens as a source of nutrients (fungus-growing termites). In the tropical regions of Africa and Asia, termites that cultivate fungi coexist in an unusual mutualism with basidiomycete fungi of the genus Termitomyces [21,47,48,50].

Since cellulose is reinforced by lignin in the higher plants' cell walls [13] preventing its bio-digestion, accordingly, the symbiotic fungi starts with disturbing lignin to ensure accessibility for the termites' own cellulose [47,51,52].

The efficiency degrading and consuming cellulose and hemicelluloses from wood by termites using wood was estimated to range from 59 to 99%. Acetate, CO_2, and H_2 are produced when protozoa or a termite's own cellulolytic enzymes directly ferment cellulose under anaerobic conditions. The acetate is subsequently absorbed by the termites, who utilize it as their primary source of oxidizable energy [21,49].

Although some organisms, like white-rot fungus and actinomycetes, have the capability of releasing the essential enzymes to break down lignin, it has been demonstrated that lignin is resistant to biochemical effects. Extracellular lignin and manganese peroxidases mediate the first reactions as illustrated by Crawford [53-61] and Kirk and Farrell [61]

It was indicated by Haug [62] that increasing lignin content in wood decreases the surface area accessible for enzymatic penetration and activity since lignin is the most resistant component of plant cell walls.

Concerning to nest constructing materials, they prepared mainly by termite themselves else from the woody-degraded residues including organic matter residues and Klason lignin as well as the earth-based materials collected and transported by these insects themselves. For the earth materials, sand, silt, loam, clay, and loose forms of soil with various levels of organic matter contents were all types of soil that the termites themselves used to build their nests [63,64]. For the woody-degraded residues, lignin polymer is the main binder used in construction of the termite nests. Similar to how lignin provides mechanical support to plant vasculature, its polymeric network that reinforces termite skeletons was reported to serve as a barrier against microbe attack and a water-tight seal [21].

White rot fungi can degrade lignin aerobically inside their cells by oxidative enzymes (ligninase peroxidase, manganese peroxidase, and laccases) faster than other organisms [65]. According to the lignin degradation theory, symbiotic fungus can degrade lignin, allowing termites' own cellulase to consume cellulose [51,52]. The absence of any known lignin-degrading bacteria in termite guts and the lack of a known location for lignin degradation both lend credence to the theory [19]. Since lignin's polyphenolic structure is more resistant than that of other wood polymers, it has long been thought to be a significant source of stable carbon in soils [66]. In addition, turnover studies of lignin revealed that large allocations of it was decomposed within a year of when embedded in soils [66]. Furthermore, Furthermore, the lignin content in older nests was found to be only half that of younger nests. These results are adapted to those indicated by Rückamp et al. [66].

 doi:10.20944/preprints202309.1492.v1

Termite nests are often rich in organic material. Given that most termite species can't degrade lignin, which was 15 times more abundant at 10 cm depth of the reference soils, lignin might be a useful tracer of the organic matter incorporated into termite nests and released into nest surrounds [67].

It was indicated that elevated lignin contents were found at 60 cm distance from the nest border as well as up to 60 cm soil depth beneath the nests. The lignin content in older nests was only half that of younger nests, and the influence on the nest surroundings was less prominent. Moreover, savanna termite *C. silvestrii* were found to enriches lignin in its earth mounds, but that only a minor part enters the soil-protected lignin fraction when nests decay, as most of the lignin is lost during nest aging [67].

It was reported that higher lignin content was discovered 60 cm from the edge of the nest and up to 60 cm into the soil beneath the nests. Older nests had lignin contents that were about half as high as those of younger nests, and their influence on the area around the nest was less pronounced. Furthermore, it was discovered that the savanna termite *C. silvestrii* enriched lignin in its earth mounds; however, only a little portion of this lignin enters the soil-protected lignin fraction when nests degrade because the majority of the lignin is lost during nest aging [67].

The crystallinity of cellulose is defined as the ratio of the amount of crystalline cellulose to the total amount of sample material including crystalline and amorphous parts. The CCs comprise different types of cellulose-based materials including microcrystalline cellulose (MCC), nanocrystalline cellulose (NCC), cellulose nanorods (CNR), cellulose nanowiskers (CNW), cellulose microfibrils (CMF), and cellulose nanofibrils (CNF) [68-76]

The MCC is pure partially depolymerized cellulose synthesized from α-cellulose precursor. The MCC can be synthesized by different processes such as reactive extrusion, enzyme mediated, steam explosion and acid hydrolysis. The later process can be done using mineral acids such as H_2SO, HCl, HBr, ionic liquids, bioenzymes. The role of these reagents is to destroy the amorphous regions remaining the crystalline domains [69].

Because of its exceptional dry binding capabilities, MCC is a beneficial ingredient in pharmaceutical applications as a tablet binder, as well as in food and cosmetic applications as an anticaking, thickener, texturizer, emulsifier, and bulking agent [69]. Moreover, due to its high strength, flexibility, and aspect ratio, MCC is also used in paints, paper and nonwoven textiles, oil field services, medicine, and composites.

The NCC is a nano-scale that having at least one dimension less than 100 nanometers in size [68]. The size, dimensions, and shape of NCCs are determined by the type of the cellulose supply as well as the hydrolysis conditions such as duration, temperature, ultrasonic treatment, and material purity [71]. In addition, regarding to its high thermal stability, NCC can be regarded as a high potential filler for industrial nanocomposite applications. The charged CNCs' particles create an anisotropic liquid crystalline phase above a certain concentration [70].

Several scientists investigated the construction and composition of termite nests referring only to their macro- and micro-scaled materials including lignin, sand, clay and organic matter contents, but no one detected the incorporation of crystalline celluloses (MCC and MCC) within the skeleton of termite nests. Accordingly, one of the current investigation' target was planned to be studied.

Many farmers and customers are suffering from infestation of their timber trees by termites, accordingly, utilization of such infected woody raw materials as a heat sink can reduce economic loss arisen from the termites' infection. According to reports, sustainability in energy recovery from biomass is becoming more appealing because biomass emits no new greenhouse gases into the environment [77,78]. Timber trees' potential as plantation species is becoming more widely acknowledged in Saudi Arabia, particularly for fast-growing species. In addition to their value as windbreaks and shelterbelts, wood is used as a source of energy through direct burning, particularly in rural locations, villages, and during Muslim pilgrimage at Mena and Araft camps, to provide heat for cooking and other traditional uses. Firewood and charcoal [77-82] are commercially marketed in various locations of Saudi Arabia at large public markets as well as traditional stores. The widespread use of firewood in Saudi Arabia stems from Saudi customs and a preference for Arabic cooking

 doi:10.20944/preprints202309.1492.v1

flavors [78]. Lignocellulosic species were argued to be better suited as fuelwood species due to their high density wood, low ash content, and low nitrogen content. Gross heat of combustion (GHC) of wood is an important property that determines suitability of such wood species for renewable energy supply. It was found a strong relationship between the GHCs of woody materials and their contents of lignin, fixed carbon, and volatile matter contents [77-82].

Since in Saudi Arabia, especially the Western region, few systematic field investigations were available only for some metropolitan few cities where grave damage have been reported on wood used in construction or infrastructure or in heavy infestation on agricultural crops, this study were conducted to investigate: 1) The most infected tree species by the small Najdian Termite, *Microtermes najdensis* located at Hada Al-Sham village Makkah Al-Mukarramah Province, 2) Studying the manner applied to adjust the internal atmosphere: temperature and ventilation (air and humidity) within the termite nest (TN), 3) Studying the mortar blend used for constructing the TN, 4) Inspiring the discovered findings to be realized in living buildings as well as be converted into novel ecofriendly natural composite products, 5) The suitability of the partially-infected wood to be used as a renewable energy resource.

2. Materials and Methods

2.1. Management Plan

Figure 1A illustrates the relationship between the termites and their surrounding's elements, namely atmosphere (Figure 1a1), soil (Figure 1a2), the tree species (Figure 1a3), their nests' skeleton (Figure 1a4). Under suitable climatic conditions (temperature and relative humidity), the termites carry out their daily activities for providing food and shelter for themselves. For the feeding issue, there is no any problem for that since they are able to digest lignocellulosic materials like wood and degrading it, along with the bio-enzymes excreted by fungus cultivated in the nest's gardens, into organic matter content (OMC) faecal materials, Klason lignin content (KLC), MCC, NCC. The termites, also, transport soil/clay particles into their nests within the infected trees and mix these ground particles with the OMC, KLC, MCC, and MCC wetting this blend with their saliva.

As shown in Figure 1B, characterization of the termite system was performed for all the four elements constituting the termites' system (Figures 1b1-1b4) for all the six host tree species that are the most susceptible trees for termite infestation as reported in (Figures 1a3) and referred at (Figure 1b3). In addition, the second step is inserting database concerning to the six tree species through four classes surrounding the termites, namely meteorological parameters, soil, healthy wood (W_h) and termite nests skeleton (TNS). Furthermore, the different essential characterizations performed for the four classes are presented in Figure 1.

Preprints (www.preprints.org) | NOT PEER-REVIEWED | Posted: 22 September 2023 doi:10.20944/preprints202309.1492.v1

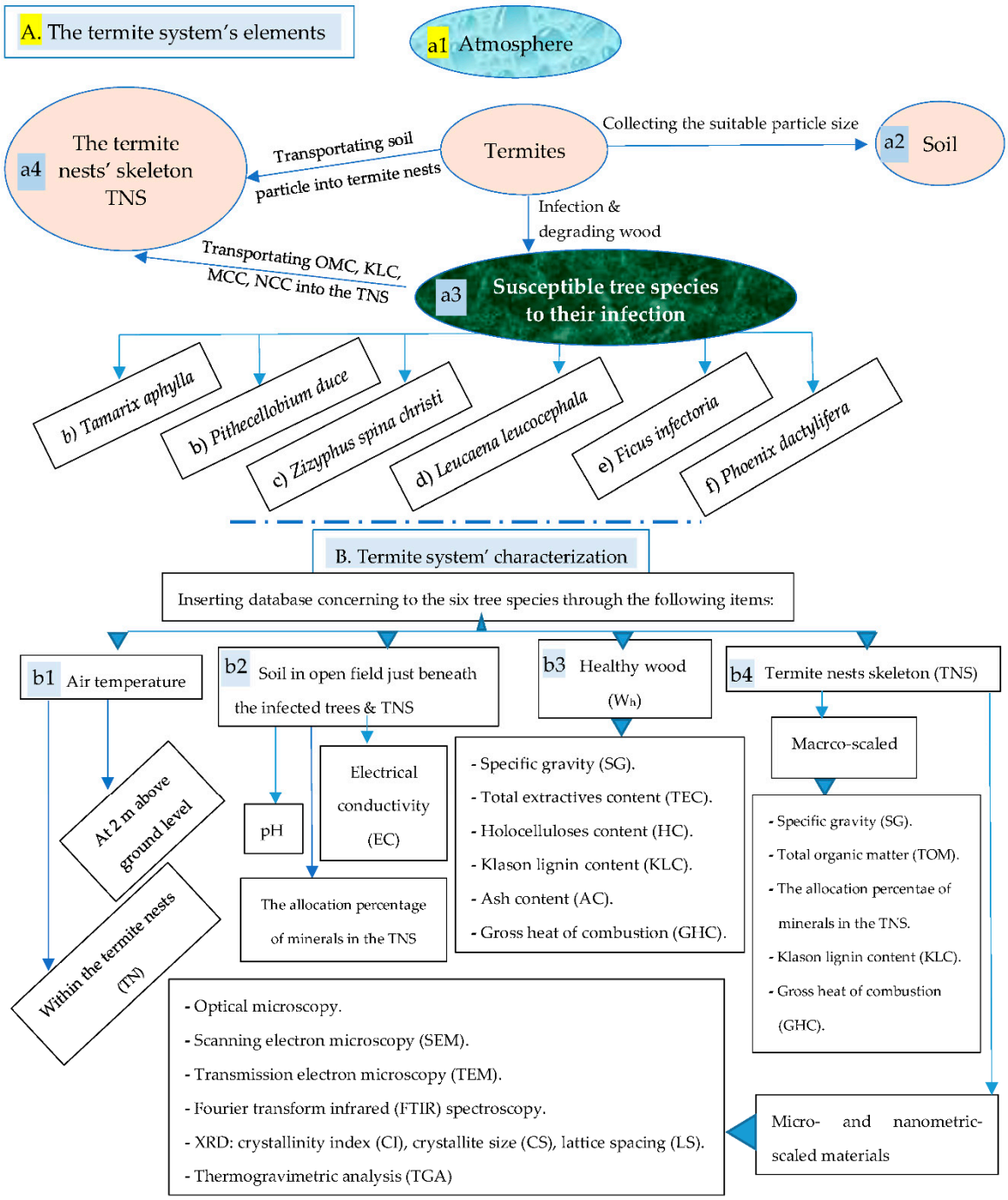

Figure 1. The management plan for: (A) studying the termite system's elements: (a1) Air temperature, (a2) Soil, (a3) healthy wood (W_h), (a4) termite nests skeleton (TNS); (B) termite system' characterization: (b1) air temperature, (b2) soil in open field and the TNS (b3) healthy wood, (b4) termite nests skeleton (TNS).

2.2. Collection and Analyzing the Termite System's Elements

The experiment was conducted at the Agriculture Research Station (ARS) of King Abdulaziz University located at Hada Al-Sham, northeast of Jeddah (21° 48′ 3″ N, 39° 43′ 25″ E), Saudi Arabia during the period extended from 01 October 2019-30 August 2020.

2.2.1. The Atmospheric Air Temperature

Preprints (www.preprints.org) | NOT PEER-REVIEWED | Posted: 22 September 2023 doi:10.20944/preprints202309.1492.v1

The dominant air temperature data of the study area were collected from the local meteorology station's saved database that was measured at a constant level of two meters above ground level.

Moreover, within termite nests, the internal atmosphere measurements were limited to air temperature recording. For this task, continuous temperature measurements were taken, daily, at specified times in six hours intervals throughout the recording period (11 months) for each of the infected trunk of *Zizyphus spina Christi* (01 October 2019-31 August 2020). The starting record was 12 am on 1 October 2019. The measurements were recorded manually using digital thermometers with chromel-alumel thermocouple probes (type K with an error of ± 1 °C). Each thermometer's probe was introduced deeply inside the termite nest passing through a naturally-holed tunnel spreading at the southwest direction. Since the pathways' gallery of the nest are not straight, an electric drill with a long steel drill bit (size 0.25 "; maximum drilling depth 10 ") was used to engrave a straight pathway for entrance the thermometer probe into the nest. It is worth for mentioning that the artificial facial opening of the nest done by the drill was closed by a binding paste such as epoxy paste or honey bees wax to prevent changing the meteorological parameters within the nest as well as preventing predators to enter to the nest.

2.2.2. Soil

The soil properties in the open field were determined [83] as well as the minerals incorporated in the mortar that termites used them during constructing their nests.

In order to prevent any termite infestation, the reference soil sites were chosen to be at least 5 m away from termite nests and did not appear to have been influenced by termites. Each sampling location had three soil transects drilled from the site's center to its four cardinal points. For each transect, samples were collected at soil depths of 10, 30, and 60 cm at a constant width of 40 cm. The soil samples present at the horizon borders were avoided and the accurate samples were about 5 cm above or below the referred borders according to Rückamp et al [67].

For the soil analysis, four random soil samples from surface layer (0-30 cm depth) were collected just beneath each infected tree chosen for this study. The collected soil samples were air dried, sieved and analyzed for different physical and chemical properties.

I. Electrical Conductivity (EC)

The EC is a measure of the amount of salts in soil (salinity of soil) that is an important indicator of soil health. The EC was measured in 1:1 soil suspension and extraction as described by Jackson [83].

II. The pH

The pH was determined in 1:1 soil suspension and extraction as described by Jackson [83].

III. Total Organic Matter Content (OMC) of Soil

The OMC present within the mortar collected from skeletons of the termite nests was done by applying loss on ignition (L_oI) method that is known to be one of the most widely used methods for this task [47,84-86]. The L_oI method was done at 450 °C during 5 h and at 600 °C during 6 h; and by the dry combustion method [85] using tube furnace (Carbolite). Since many factors may influence accuracy of this determination process such as furnace type, sample mass, duration and temperature of ignition and clay content of samples [47,84,85], all these factors were standardized for all the tests.

V. Total Minerals Content in Soil (open field)

2.2.3. The Healthy Wood (W_h)

The most susceptible tree species to infection by Najdian termite, *Microtermes najdensis* located at Hada Al-Sham village, KSA were chosen from the enormous species habituating and cultivated in the KAU farm to study the termite infection as well as their susceptibility to the termite attack. These species were *Tamarix aphylla* (L.) H.Karst. (Family: Tamaricaceae Link), *Pithecellobium dulce* (Roxb.) Benth. (Famiy: Fabaceae Lindl.), *Ziziphus spina-christi* (L.) Desf. (Famiy: Rhamnaceae Juss.), *Leucaena leucocephala* (Lam.) de Wit (Famiy: Fabaceae Lindl.), *Ficus infectoria* Roxb. (Famiy: Moraceae Gaudich.), and *Phoenix dactylifera* L. (Arecaceae Bercht. & J.Presl). Three trees were selected from each

species representing three replicates. Both the first and the latest genus (tamarix and Phoenix) are native to Saudi Arabia, while the other four genera were not.

After selecting the six tree species, wood samples was prepared for the healthy wood (W_h), and the termite nests' skeleton (TNS) as illustrated in Figures S1a, and S1b, respectively.

A disc (approximately 30 cm thick) was sawn from each tree at a height of 0.6 m or so, and it was used to determine the wood's qualities. One bolt (approximately 1.8 cm tangentially and 30 cm long) was sliced longitudinally after the pith was isolated. Each inner- and outer-wood zone of each bolt had a diametric strip (nominal 1.8 cm tangentially and radially, and 30 cm longitudinally) removed. Accordingly, each bolt yielded two diametric strips. As a result, the removed strip was afterwards crosscut into four imperfection-free cubic samples according to Hindi [82].

The remaining volume of the wood disc, else inner or outer wood zones were separately converted into meal. Then, based on the standard methods for determining wood quality, wood meal was screened using various standard sieves and specified for the determinations of total extractives content (TEC), lignin content (KLC), holocelluloses content (HC) and ash content (AC) of the six lignocellulosic materials.

Three samples were randomly selected from each tree (a total of 9 samples of the three trees specified for each species) for each determination. For the six wood resources that were employed for each determination, 54 samples were accordingly specified.

Concerning to the characterization, the samples were prepared as indicated at Figures 1, and S1. The following wood properties were considered and their values were calculated as shown in Table 2:

I. The Specific Gravity (SG) of the W_h

The SG of wood was determined by using Pycnometric displacement of water based on oven-dry weight and saturated volume.

Five defect-free samples (2.5 cm radially and tangentially and 2 cm longitudinally each) were used from each tree (15 samples of each species). Accordingly, 90 samples were specified for the six tree species used. The green samples assigned for this test were accurately re-saturated by water under vacuum and the saturated volume was measured by Pycnometric displacement of water. The SG was calculated based on oven-dry weight and saturated volume [87] as presented at Table 1.

II. Total Extractives Content (TEC) of the W_h

The TEC of the healthy wood (W_h) was determined according to the ASTM [88]. Each sample assigned for extractive content determination was about one gram of an air-dried wood meal that has been' ground to pass through a No. 60 (250 urn) sieve and be retained on a No. 80 (180 um) sieve. The samples were extracted in a Soxhlet apparatus with ethanol-benzene mixture (in ta ratio of 1:2) for 4 hours, followed by extraction with 95 %ethanol for 4 hours, then extraction with a hot deionized water for 3 hours with changing of water every one hour . The extracted sample was oven-dried to a constant weight at 103 ± 2°C, and the TEC was calculated using the formula presented at Table 1.

III. Holocelluloses Content (HC) of the W_h

The combination of hemicelluloses and alpha cellulose makes up the HC of wood [89]. According to the methodology outlined by Wise et al [90] and Hindi [12], it was determined as follows: A five weight percent fiber solution was made and combined with 0.75 g of sodium chlorite and 0.5 mL of glacial acetic acid. The temperature was held at 75 °C for one hour while the flask was top sealed to prevent the loss of gas generated during the reaction process. The chemical reagents were changed twice. The HC of wood was calculated as presented at Table 1.

IV. Klason Lignin Content (KLC) of the W_h

The approach used by Hindi [68] and described by ASTM [91] and Jayme et al. [92] was used to determine the KLC. The diluted sulfuric acid solution (72%) was used to hydrolyze the extractives-free wood sample at 35°C. The sample was secondarily-hydrolyzed for 30 minutes after being primarily-hydrolyzed for an hour using 200 ml of distilled water. Whattman filter paper No. 44 was used to filter the material, which was then dried by air, oven, and weight. The KLC was determined as clear in Table 1.

V. Ash Content (AC) of the W_h

 doi:10.20944/preprints202309.1492.v1

The ASTM [84,87] was used to determine the AC of wood. The wood meal samples weighing about 2 g each that had been ground to pass through a No. 40 (425 um) sieve were gathered. Each sample was put into a porcelain crucible, dried in an oven at 103 ± 2 °C to a constant weight, and then weighed. In a tube furnace, the exposed crucible containing the sample was lit at 600 °C until all the carbon was burned off. It was then weighed after cooling in the desiccator. Up until the weight after cooling is constant to within 0.2 mg, the heating was repeated at 30 minute intervals. Based on the weight of the oven-dry wood meal, the proportion of residual containing ash was estimated (Table 1).

VI. Gross Heat of Combustion (GHC) of the W_h

After preparing the GHC's specimensas clear at Figure S1. the GHC of each of the healthy wood and the TNS was determined using an adiabatic oxygen bomb calorimeter, Parr 1341 in accordance with the ASTM [93] as well as the procedures stated by the Parr instruction manual as explained at Figures 1, S1, and S3. The W_h samples were prepared according to the flowchart presented at Figure 1. Using a pellet press, model Parr 2811, each sample (0.8 g) designated for measuring GHC was formed into a pellet. The samples were dried in an oven and weighed. The calorimeter was calibrated using pellets of benzoic acid. Under carefully regulated circumstances, the sample was inserted in a metallic capsule and exploded within the oxygen bomb Parr 1108.

Using a mercurial thermometer (Parr 1603), temperature observations were recorded before, during, and after combustion. On a moisture-free basis, the heat generated by a sample's combustion was estimated and converted into calories per grams. The estimates for the GHC included correction factors for the combustion of fusing wire and thermometer. On the other hand, because they are too minor to take into account, correction factors for the generation of nitric and sulfuric acids were not included in these calculations [94] and you can understand these calculations with their corrections through Table 1.

2.2.4. Sampling and Characterization of the Termite Nests Skeleton [TNS]

It was assumed that the majority of nests were built around mid of 2019/2020. In order to select the infested tree species and determining the termite nests' locations within the trees, intensive monitoring of all lands within the ARS. The nests included numerous passageways and galleries with dense walls made primarily of organic residues arisen essential from the infested woody trees themselves as well as earth material transferred from beneath the infested trees-bearing the termite nests (Figure 3). Due to the majority of their apertures being on the western side, the nests appeared more wormer than the outer surrounding climate. For sampling, three replicates of each nest as well as reference soils were chosen according to Al-Ghamdi et al. [7] and Faragalla and Al Qhtani [8].

Termite nests were sampled at about 50 cm above the ground level. At each location, five 100 cm^3-cores were used for the sampling process as explained at Figure S1b. Every sample was promptly air dried after collection. Regarding to physical and chemical characterization, the following properties were considered for the TNS:

2.2.4.1. Specific Gravity (SG) of the TNS

This SG, here, was determined in a dryness circumstance to keep the TNS' construction to be intact as it is in the virgin termite nests without altering its SG.

Samples of the TNS were oven-dried to a constant weight at 103°±2 °C and weighed. Then, the oven-dry volume of each sample was determined by using Amsler volume meter filled with pure mercury. The SG of the TNS was calculated based on oven-dry weight and volume (Table 1).

2.2.4.2. Klason Lignin content (KLC) of the TNS

The KLC of the TNS was determined using the same KLC's technique applied for the W_h samples, except for some modifications due to the difference between both materials (TNS and W_h) in their nature. Before determination of KLC of the TNS sample, its content of sand, ash and the organic matter other than lignin were discarded to get the pure KLC. For the sand particles, they were

 doi:10.20944/preprints202309.1492.v1

removed by saturation of the sample in a suitable amount of distilled water under fast stirring using and, after that the liquor was vacuum-filtered. The KLC of the TNS was calculated based on oven-dry weight (Table 1).

2.2.4.3. Total Organic Matter Content of the TNS

2.2.4.4. Total Minerals Content of the TNS

By thermal elimination of TOM, and we can estimate the minerals by subtraction. After sieving to ~2 mm and subsequent grinding with a ball mill, organic carbon (OC) was measured with an elemental analyzer (NA 2000, Fisons Instruments, Rodano, Milan, Italy). The minerals of some selected samples were characterized by X-ray diffraction (PW 1130, Philips, Almelo. The Netherlands).

2.2.4.5. Gross Heat of Combustion (GHC) of the TNS

The GHC of the TNS was determined using the same adiabatic oxygen bomb calorimeter used for the W_h. In addition, its samples' preparation was applied according to Figure S1b, while its calculations with their corrections was illustrated at Table 1.

2.2.4.6. Mechanical Properties of the TNS

Specimens the TNS were used to examine strength of the TNS to best suggestion of using such TNS' blend as a bioinspired composite materials in building sectors, especially at rural villages and tourist regions. Each TNS mass (see Figures 7, S1) was sectioned into slices and samples were extracted from each slice according to Zachariah [95].

The stress–strain behaviors of the TNS collected from six infected tree species were measured using Instron universal testing machine, model 1193, Instron Co., Ltd., London, UK, with a 200 N-load cell according to the ASTM D–882 standard test, 1989. The device with two metallic grips was installed to hold the test sample at both ends. The starting grip separation for all samples was 50 mm, and the upper grip was extended at a constant rate of 50 mm per minute while the lower grip remained stationary. An automatic speed controller was fitted to the electrically powered machine to maintain the upper grip's speed. The ambient temperature was used for all measurements. From the plot of stress–strain curves, the mechanical properties, namely, ultimate tensile strength (UCS) in MPa, modulus of elasticity (MoE) in MPa, and deformation at failure (EaF) as a percentage, were calculated (Table 1).

The ultimate compressive strength (UCS) of the TNS shows its maximum allowable compressive stress [-]. The UCS property was calculated by dividing the maximum load causing the failure of the TNS by the cross-sectional area of the specimen, as explained in Table 1.

The modulus of elasticity (MoE) is a reliable indicator of the TNS' stiffness. The MoE was computed by dividing the stress at yield by length of the TNS' specimen at yield, as expressed in Table 1.

Concerning to the deformation at failure (DaF) it was calculated by dividing the deformation at failure of the TNS' specimen by the initial gauge length, as shown in Table 1.

Preprints (www.preprints.org) | NOT PEER-REVIEWED | Posted: 22 September 2023 doi:10.20944/preprints202309.1492.v1

Table 1. Calculation of different chemical and physical properties of the lignocellulosic resources used for construction of the termite nests found at Hada Al-Sham, Saudi Arabia.

Equation	Definitions
[1] MC_{hw}, % = $[(W_{adhw} - W_{odhw}) / W_{odhw}] \times 100$ [2] MC_{tns}, % = $[(W_{adtns} - W_{odtns}) / W_{odTNS}] \times 100$ [3] $SG_w = W_{odhw} / V_{shw}$ [4] $SG_{tnm} = W_{odtns} / V_{odTNS}$ [5] AC, % = $(W_a / W_{efhw}) \times 100$ [6] TEC, % = $[(W_1 - W_2)/W_1] \times 100$ [7] HC [8] KLC, % = $(W_{lr} / W_{efw}) \times 100$ [9] TOMS, % = [10] TOMN, % = [11] TMS, % = [12] TMN, % = [13] GHC, calories/g = $[(t\ E_e) - e_1 - e_2 - e_3] / W_{odhw}$ or W_{odTNS} [14] $t = t_c - t_a - r_1 (b-a) - r_2 (c-b)$ [15] $e_1 = = c_1$ if 0.0709N alkali was used for the titration. [16] $e_2 = (13.7 \times c_2)(W_{odhw}$ or $W_{odTNS})$ [17] $e_3 = 2.3 \times c_3$ [18] $r_1 = (T_a - T_b) / 5$, calories/min. [19] $r_2 = (T_d - T_e) / 5\}$, calories/min. 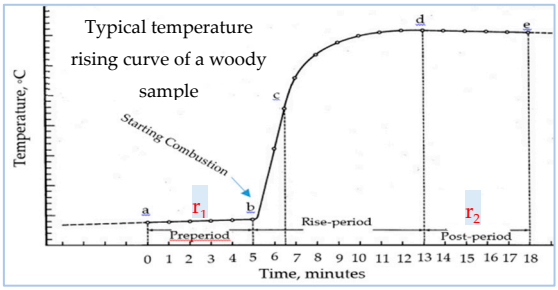	W_{adhw}: Weight of air-dried healthy wood , g. W_{odhw}: Weight of oven-dried healthy wood, g. W_{adTNS}: Weight of air-dried termite nest skeleton (TNS), g. W_{odTNS}: Weight of oven-dried termite nest skeleton (TNS), g. V_{shw} = Volume of water-saturated healthy wood, cm^3. V_{odTNS}: Volume of oven-dried TNS, cm^3. W_{ahw}: Weight of ash matter of healthy wood. W_{efhw} = Weight of extractive-free oven-dried healthy wood meal, g. W_{lr}: Weight of lignin residues, g. W_{OMS}: Weight of total organic matter in soil (open field), g. W_{OMN}: Weight of total organic matter in TNS, g. W_{MS}: Weight of minerals in soil (open field), g. W_{MN}: Weight of minerals in nest, g. GHC: Gross heat of combustion, calorie/g. E_e = Energy equivalent of the calorimeter, determined under standardization e_1: Thermochemical correction in calories for heat of formation of nitric acid (HNO_3). e_2: H_2SO_4. e_3: Thermochemical correction in calories for heat of combustion of fuse wire. a: Time of combusting the sample. b: Time (to nearest 0.1 min.) when the temperature reaches 60 % of the total rise in temperature. c: Time at beginning of the post-period, whereby the rate of temperature change has become constant. c_1: milliliters of standard alkali solution used in the acid titration c_2: sulfur content in the sample, %. c_3: centimeters of fuse wire consumed in firing. T_a: Temperature at time of combusting the sample T_b: Temperature at time of combusting the sample. T_c: Temperature at the point c (See the temperature rise curve, at the left side°°). T_d: Initial temperature at the final period after combusting the sample. T_e: Final temperature at the last period after combusting the sample. r_1: rate (temperature units per minute) at which the temperature was rising during the 5-min. period before combusting the sample. r_2: rate (temperature units per minute) at which the temperature was rising during the 5-min. period after time, where r_1 and/or r_2 = '+' when the temperature is rising and '-'when the temperature is falling.
[20] $C_s = K\lambda/\beta_{1/2}\text{Cos}\ \theta$ [21] $L_s = n\lambda / 2\sin\theta$	K: The correction factor and usually taken to be 0.91 λ: The radiation wavelength of X-rays incident on the crystal (0.1542 nm). θ: The diffraction angle. $\beta_{1/2}$: The corrected angular full width at FWHM. FWHM: The full width at half maximum of a XRD- peak. n: An ordinal number taking a value of "1" for diffractograms having the strongest intensity.
[22] Compression strength = F_f/A [23] MoE = Stress/Strain at the PL = σ/ε [24] $\varepsilon = [\Delta L/L_o] = [(Lf - L_o)/L_o]$ [25] EaF = $\Delta Lf = [(Lf - L_o)/L_o] \times 100$	F_f : Force at failure in Newton (N). A: Cross-section area (m^2) of the Termite nest skeleton. σ: Compression stress (Pa). L_f : The length of the Termite nest skeleton at failure. L_o: The initial length of the Termite nest skeleton at failure.
[26] $d = W_{odTNS} / V_{odTNS}$ [27] $P = 1 - (d/d_p)$	d_p: Density of non-porous.

[1] Moisture content of healthy wood; [2] Moisture content of termite nest skeleton; [3] Specific gravity of healthy wood; [4] Specific gravity of termite nest skeleton; [5] Ash content of healthy wood; [6] Total extractives content of healthy wood; [7] Holocelluloses content of healthy wood; [8] Klason lignin content of healthy wood; [9] Total organic matter in soil; [10] Total organic matter in TNS; [11] Total minerals in soil; [12] Total minerals in TNS; [13] Gross heat of combustion of healthy wood; [14] Temperature rise; [15] Correction for heat of formation of nitric acid; [16] Correction for heat of formation of sulfuric acid; [17] Correction for heat of formation of the nickel chromium-fuse wire; [18] Temperature rate for preperiod of combustion; [19] Temperature rate for post-period of combustion; [20] Crystallite

 doi:10.20944/preprints202309.1492.v1

size, nm using Scherer equation with respect to the crystallographic plane (CP) of '002'; [21] Lattice spacing, nm using the Bragg's equation at CP of 002; [22] Tensile strength (MPa), [23] Modulus of elasticity (GPa), [24] Tensile strain, [25] Elongation at failure (%); [26] Real density of the TNS; [27] Porosity.

The Micro- and Nanometric-Scaled Materials

Microcrystalline Cellulose (MCC) represents the micrometric-scaled polymeric materials in the termite nest skeleton (TNS), while nanocrystalline cellulose (NCC) is the famous nanoparticles assemblies the TNS that were discovered for the first time throughout humanity's history.

Characterization

MCCs and NCCs samples were assigned to XRD, FTIR, SEM and TEM investigations. For the XRD, FTIR, since their micrometric-scaled samples must be a fine powdered form, they were ground in a ball mill to passes through a 100 mesh and be retained on a 120 mesh. On the other hand, for each of the MCC and NCC samples specified for SEM and TEM spectroscopic studies, a thin film of each individual solution was required for each characterization. This solution was prepared from each powder type that was completely dissolved in an absolute ethanol by assistance of sonication.

I. Scanning Electron Microscopy (SEM)

SEM study was used to study the surface morphology and types of anatomical features in the tangential plane samples of leaflet tissue as well as the SCNCs. The samples were placed on the double side carbon tape on Al-stub and dried in air. Before examination, all samples were sputtered with a 15 nm thick gold layer [JEOL JFC- 1600 Auto Fine Coater] in a vacuum chamber. The sample s were examined with a SEM Quanta FEG 450, FEI, Amsterdam, Netherland. The microscope was operated at an accelerating voltage ranged from 5-20 kV.

II. Transmission Electron Microscopy (TEM)

This characterization was examined by TEM (JEM-1011 JEOL, Japan). The suspension was sampled by using a capillary pipet and dropped onto the copper grid. After being dried for 3 min at ambient condition, filter paper was used to remove the excess liquid on the copper grid. Afterwards, the dye liquor of phosphotungstic acid was dropped and dyed for 2 min. The dried sample was prepared for observed. The operated voltage was at 100 kV.

III. Fourier Transform Infrared (FTIR) Spectroscopy

Chemical structure (functional groups) of the parent alpha as well as the cellulose-based products (MCC and NCC) were investigated by the FTIR using a Bruker Tensor 37 FTIR spectrophotometer. The samples were oven-dried at 100°C for 4-5 h, mixed with KBr in a ratio of 1:200 (w/w) and pressed under vacuum to form pellets. The FTIR-spectra of the samples were recorded in the transmittance mode in the range of 4000-500 cm^{-1} [70,71].

IV. The X-Ray Diffraction (XRD)

The X-ray powder diffraction spectra of the fibers were used to study the crystallinity of the using the XRD-D_2 Phaser Bruker (USA). The generator was operated at 30 KV and 30 mA. The samples were exposed for a period of 3000s using CuKa radiation with a wavelength of 0.15418 nm. All the experiments were performed in the reflection mode at a scan speed of 4° /min in steps of 0.05°. All samples were scanned in a 2θ=26° range varying from 4° to 30°. The crystallinity index individual crystalline peaks were first extracted by a curve-fitting process from the diffraction intensity profiles [70,71,97]. The CI was calculated by dividing the diffractogram area of crystalline cellulose by the total area of the original diffractogram. The area under the curve was estimated by summing of adjacent trapezoids using Excel (Microsoft, USA) as indicated by Hindi [70,71,93].

Statistical Design and analysis

Differences between groups were examined with an analysis of variance (ANOVA), and the LSD0.05 test for comparisons of the mean values. The significance level was set at $P < 0.05$. The ANOVA was conducted with SPSS 14.0 (SPSS Inc., 2005, Chicago, USA) as illustrated by El-Nakhlawy [98].

3. Results and Discussion

3.1. Climate

 doi:10.20944/preprints202309.1492.v1

3.1.1. Climate at Hada Al-Sham

Concerning to the most important parameters dominant at Hada Al-Sham region collected from the local meteorological station, their mean values were presented at Table 2. Since January was the coldest month throughout the investigation period (October 2019-August 2021) that stresses termites due to low temperatures, the meteorological data of this month are presented at Table 2.

Table 2. Climate at Hada Al-Sham: Air temperature (AT), soil temperature (ST), income and outcome radiation for each of shortwave and longwave, wind speed (WS), wind direction (WD), barometric pressure (BP) during January 2021.

Property	Height	Mean	Max	Min
Air temperature, ◦C at:	2 m	24.69	33.29	14.56
	5 m	24.75	32.7	15.85
	10 m	22.63	63.91	-0.683
Soil temperature at 50 cm, °C		28.79	31.37	27.93
Radiation wavelength	Income shortwave	33.79	143.3	-0.029
	Income longwave	6.26	41.76	-9.39
	Outcome shortwave	184.53	837	-6.451
	Outcome longwave	-42.579	-3.387	-84.1
Wind speed at 10 m, m/sec		2.38	11.66	0
Wind direction at 10 m, degrees		159.52	353.6	0.071
Barometric pressure, mbar		988.08	993	983

[1] N=1492.

3.1.2. Internal Temperature within the Termite Nests

Concerning to the conditioning status within the termite nest, the internal temperature (IT) of the nest and the outer temperature (OT) of the surrounding atmosphere were monitored, measured and plotted against time in six hours intervals during the period extended from October, 2018 up to the end of August 2020 as shown in Figure 2.

The eleven months included for the temperature measurements were October 2019, November 2019, December 2019, January 2020, February 2020, March 2020, April 2020, May 2020, June 2020, July 2020, and August 2020 as shown in Figure 2.

The obtained histograms matched the historical temperature data in which the minimal values of January is the coldest month, and the months from October to April are colder than the summer months. This thermal behavior adapted that resulted at Figure 3.

Preprints (www.preprints.org) | NOT PEER-REVIEWED | Posted: 22 September 2023 doi:10.20944/preprints202309.1492.v1

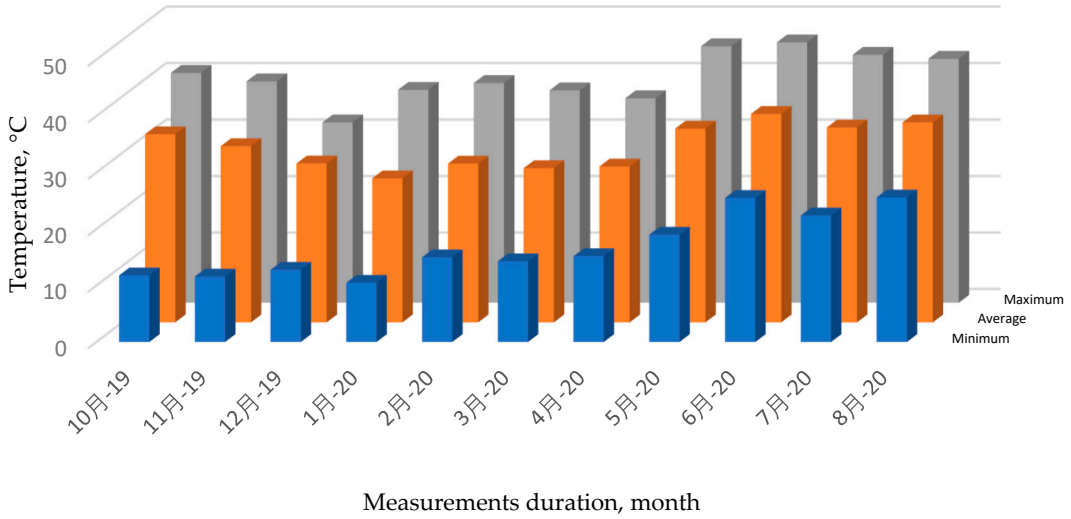

Figure 2. Temperature parameters (minimum, average, maximum) of the interior within the termite nests engraved naturally within the infected trunk of *Zizyphus spina Christi* grown at Hada Al-Sham village.

The IT was found to be milder than those for their analogous values for the outer environment, namely outer temperature (OT). For more simplifying, the IT was wormer than OT during cold durations, while it was colder than the hottest OT in hot days and vice versa [99,100]. Moreover, the IT wax exceeded more than its average level towered higher temperatures. This response is identical for all the eleven graphs representing the 11th months of the measuring period. This common trend indicates that termites prefer wormer atmospheres other than the colder one, that is expected that coldest nest may affects termite members' activity, especially their youngs.

Preprints (www.preprints.org) | NOT PEER-REVIEWED | Posted: 22 September 2023 doi:10.20944/preprints202309.1492.v1

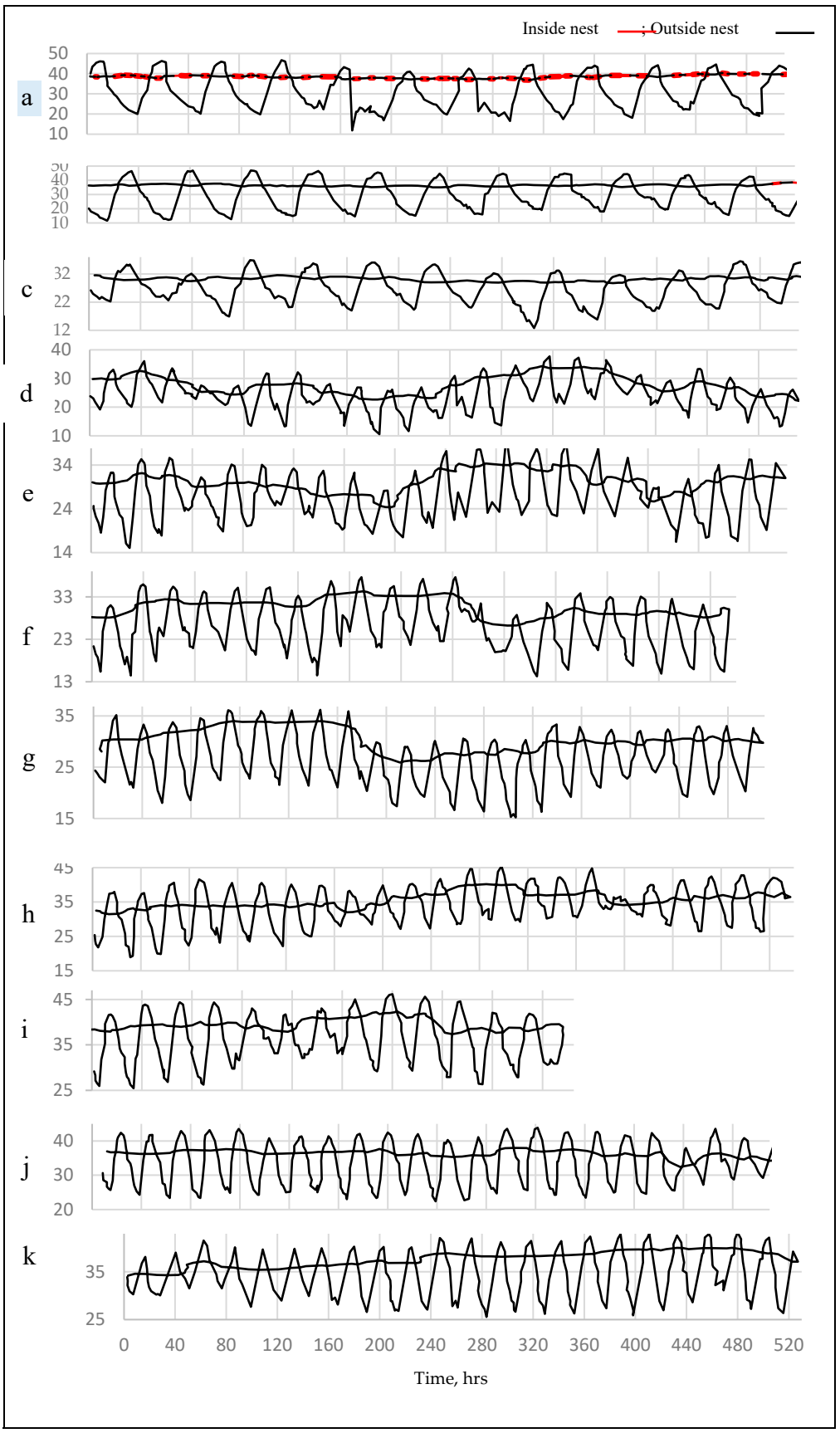

Figure 3. Mean values of temperature measurements (T, °C) of the air about 2 m above the ground level, (—),the zigzag line and inside the termite nest, the slightly waved line (------) throughout eleven months (October-August) during 2019-2021 for the open atmosphere and within the termite nests engraved in the infected trunk of *Zizyphus spina Christi* grown at Hada Al-Sham village, Makkah Province, Saudi Arabia (each value is an average of two observations: The starting record is 12 am):

 doi:10.20944/preprints202309.1492.v1

(a) October 2019, **(b)** November 2019, **(c)** December 2019, **(d)** January 2020, **(e)** February 2020, **(f)** March 2020, **(g)** April 2020, **(h)** May 2020, **(i)** June 2020, **(j)** July 2020, **(k)** August 2020.

3.2. *Soil*

3.2.1. Physical and chemical properties [101,102]

Clay, silt and sand contents, texture class, bulk density, air porosity, organic matter content (OMC), EC, and pH of the soil collected just beneath the six infected tree species are presented at Table 3.

Table 3. Initial physical and chemical analyses of the virgin soil surrounding the infected sites that would be used by termites to construct their nests.

Variables	Valuem %
Clay %	9.7
Silt %	15.5
Sand %	74.8
Texture class	Sandy loam
Bulk density (g/cm^3)	1.87
Air porosity (%)	29.4
Organic matter (%)	0.65%
EC [1:1 soil extraction] ($dS\ m^{-1}$)	0.366
pH (1:1 soil suspension)	7.70

3.2.2. Particle Size Distribution of the Parent Soil

It can be seen from Figure 4 that the parent soils collected outside the termite nests just beneath each tree of the six species have highest fractions of the coarse particles [> 425μ] for both *Tamarix nilotica* and *Zizyphus spina Christ*. On the other hand for the other four species sites, their major soil particles fractions are between 125-300 μ followed those higher than 425 μ. It was think that using coarser soil particles in the mortar blended with fine particles of organic materials, lignin and nanocellulose (MCC, NCC) allow to fabricate more permeable TNS featured by its high gas exchanging.

Preprints (www.preprints.org) | NOT PEER-REVIEWED | Posted: 22 September 2023 doi:10.20944/preprints202309.1492.v1

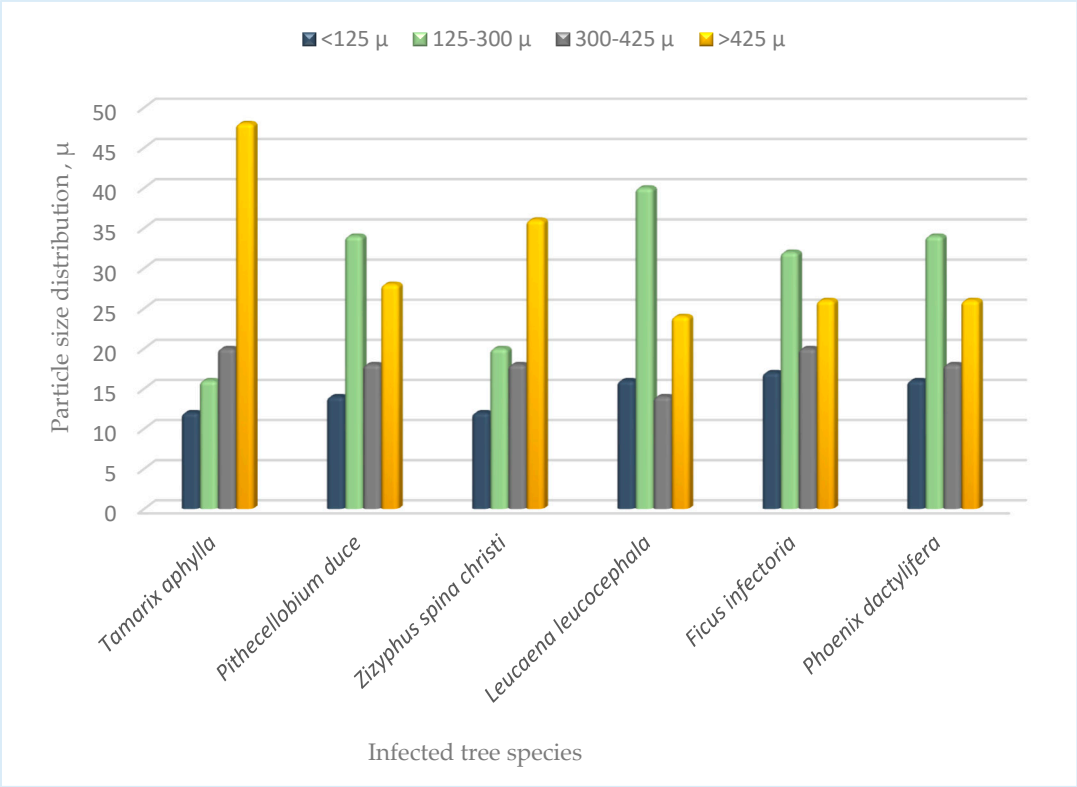

Figure 4. Particle size distribution of the parent soil just beneath each of the six infected tree species.

3.2.3. Electrical Conductivity (EC) of Soil

It can be seen from Figure 5 that EC of the soil particles used to construct the termite nest was found to be higher than that for the parent soil collected just beneath each of the six infected tree species.

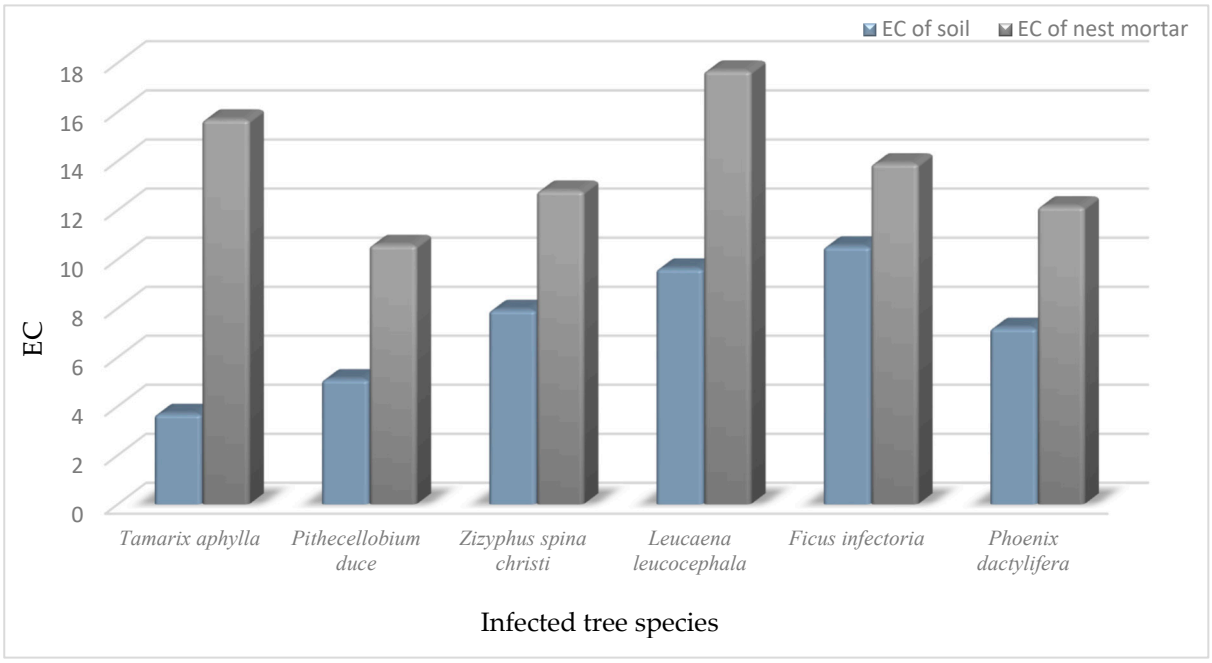

Figure 5. Electrical conductivity (EC) of the parent soil just beneath the infection sites and the termite nest skeleton (TNS) occupied trunks of the six tree species.

Preprints (www.preprints.org) | NOT PEER-REVIEWED | Posted: 22 September 2023 doi:10.20944/preprints202309.1492.v1

3.2.4. Calcium Carbonate in the Parent Soil

$CaCO_3$ compound is found naturally in the soil composition, else that belonging to the open field close to the infected tree or those collected from the nest mortar used to blend the TNS. Since this chemical compound is well known by its binding behavior, termites extract it from soil using it to enhance the TNS' rigidity without reducing the TNS' porosity.

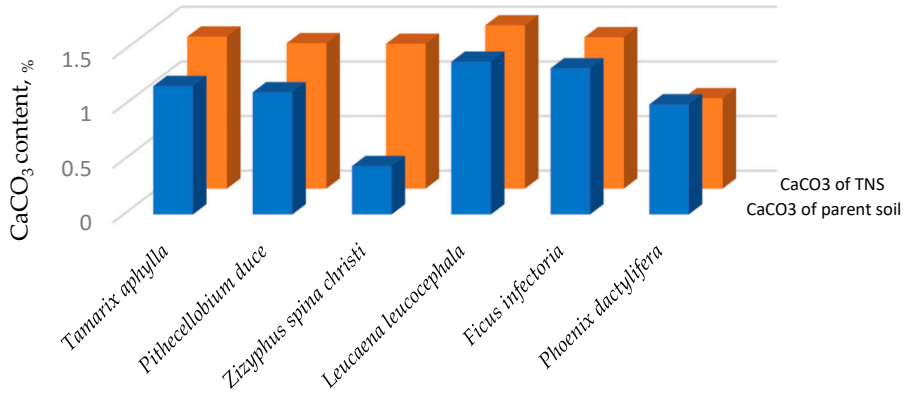

Figure 6. Calcium carbonate content of the parent soil surrounding infection sites and the termite nest skeleton (TNS) occupied trunks of the six tree species.

3.3. The Healthy Wood (W_h)

The physical and chemical properties of the W_h were investigated and are presented in Table 4. Statistical analysis showed a significant difference between the six infected tree species tested concerning all the properties examined and presented at Table 4.

Regarding to the specific gravity (SG) of the W_h, it was found that SG varied significantly due to natural resources effect. The SG means ranged from 0.42 for *Phoenix dactylifera* to 0.71 and 0.72 for *Tamarix aphylla* and *Conocorpus erectus* wood, respectively. Moreover, the remaining tree species were occupied a median level of the SG's scale. (Table 4). Lower SG values indicate that their cell wall backbone is expected to be penetrated by termites more easily digesting its carbohydrate contents comparing to the other lignocellulosic tissues with higher SGs.

Concerning to the ash content (AC) of wood, the woody polymeric tissues examined in the present investigation were significantly different in their contents of ash. Two resources of them contained the highest AC value (6.71 % and 5.43 %, for *Tamarix aphylla and Phoenix dactylifera*, respectively) comparing to the other species (Table 4). On the other hand, the other four infected species had lower AC values ranging from 1.22 % to 3.8 %. According to the continuous monitoring of study area at Hada Al-Sham region, termites infected the six hardwood species irrespective of their contents of ash as clear from Table 4. Concerning to the partially-infected wood, it must be directed to any economical applications. It is worth for mentioning that the chemical recovery application will be significantly impacted by high ash concentrations, which could be a significant disadvantage [103]. The findings, however, agreed with those found in other publications.

The six infected lignocellulosic resources examined varied significantly from one resource to another concerning to the TEC property. The highest TEC value were resulted for *Zizyphus sp.* as well as the date palm wood (18.89 % and 18.3 %, respectively), followed by the *Tamarix sp*. (15.76%). On the other hand, *Pithecellobium duce* had the lowest TEC value among the six infected woods as clear in Table 4. The extractives' content of wood don't considered as a determining factor for wood infection by termites since all the six species studied were infected in a similar manner and probabilities despite of their differences in the TEC contents. On the other hand, when searching about the possibility of using the partially-infected wood in a certain industrial application such as fiber production and/or a domestic utilization such as firewoods, the presence of high extractives into the lignocellulosic

Preprints (www.preprints.org) | NOT PEER-REVIEWED | Posted: 22 September 2023 doi:10.20944/preprints202309.1492.v1

tissues is unpreferred in the industrial sector due to their interference with the chemical reagents used in that application [103]. Accordingly, the TEC of wood must be organic solvent-extracted before manufacture, thus step will add additional cost to this industry.

Regarding to the holocellulose content (HC) of wood, the studied natural resources were found to be significantly different. Examining Table 4 revealed that *Leucaena leucocephala* and *Pithecellobium duce* had the highest values (70.82 % and 69.41 %, respectively). On the other hand, *Tamarix aphylla* and *Phoenix dactylifera* had the lowest HC values (51.8 and 53.57, respectively). In between, *Zizyphus sp*. and *Ficus infectoria* hadan intermediate situation (59.5 % and 61.59 %, respectively) concerning to the HC of the healthy wood. Accordingly, it can be suggested for the fast growing species, *Leucaena leucocephala*, that its partially-infected wood can be used as cellulose derivatives and/or as lignocellulosic fibers for fiber-reinforced composite materials or papermaking applications [103,104].

The finding belonging to Klason lignin content (KLC), it can be seen from Table 4 that both *Tamarix aphylla* and *Ficus infectoria* contained the highest KLC values (27.9 % and 22.43 %, respectively). On the other hand, *Leucaena leucocephala* had the lowest KLC content (18.86 %). In between, *Pithecellobium duce* and *Zizyphus spina christi* were similar statistically in their KLC content (20.3 % and 19.71 %, respectively) and occupied a median level within the species studied.

The results are in agreement with those encountered in annual plants, non-wood hardwood and softwood sources that found by other researchers [103, 104].

The partially-infected timber trees are more suitable for reusing in fiber production as well as renewable energy resources comparing to the date palm species although the later the most abundant raw material in Saudi Arabia. The best resource is *Leucaena leucocephala* because of its high holocellulose content, appropriate fiber length, and specific gravity that is similar to that of hardwoods. In comparison to the other resources we looked at, it has less lignin, ash, and total extractives. In addition, compared to other woody raw materials, lignocellulosic materials with low lignin content have shorter pulping times and lower chemical charges [105-106]. Additionally, it is anticipated that the pulp industry will use more chemicals at greater lignin contents [107].

Examining Table 4 for the gross heat of combustion (GHC), it can be observed that the GHC was ranged from 4102 cal/g to 4814 cal/g, for *Phoenix dactylifera* and *Zizyphus spina Christi*, respectively. These values of the intact woody specimens (W_h) lies with the traditional scale and we can suggest their utilization as renewable energy resources [78]. Based on this benefit, it can be suggested that partially-infected wood can be directed to the energy sector to generate heat for domestic and industrial applications. In addition, this utilization help to discard any traces of this dangerous insects.

Table 4. Mean values [1,2] for specific gravity (SG), ash content (AC), total extractives content (TEC), holocelluloses (HC), Klason lignin content (KLC) and gross heat of combustion (GHC) of wood samples taken from healthy trees of the six species.

Species	SG[3] g/cm^3	AC[4] %	TEC[4] %	HC[4] %	KLC[4] %	GHC calories/g
Tamarix aphylla	0.71 ± 0.04	5.43 ± 0.048	15.76 ± 0.35	51.8 ± 2.08	27.9 ± 0.56	4393 ± 91.3
Pithecellobium duce	0.61 ± 0.02	3.8 ± 0.08	6.91 ± 0.31	69.41 ± 2.34	20.3 ± 0.45	4763 ± 102.7
Zizyphus spina christi	0.72 ± 0.018	1.9 ± 0.02	18.89 ± 0.32	59.5 ± 2.42	19.71 ± 0.61	4814 ± 105.4
Leucaena leucocephala	0.59 ± 0.03	1.22 ± 0.02	9.74 ± 0. 34	70.82 ± 1.73	18.86 ± 0.14	4206 ± 86.7
Ficus infectoria	0.54	2.44	10.54	61.59	25.43	4367

Preprints (www.preprints.org) | NOT PEER-REVIEWED | Posted: 22 September 2023 doi:10.20944/preprints202309.1492.v1

	± 0.032	± 0.018	± 0.26	± 2.85	± 1.31	± 78.4
Phoenix dactylifera	0.42 ± 0.015	6.71 ± 0.71	18.3 ± 0.42	53.57 ± 2.29	22.43 ± 1.07	4102 ± 82.49

[2] Each value is an average of 5 samples. [3] Based on oven-dry weight and green volume. [4] As percentage of oven-dry wood weight. [103-110]

3.4. The Termite Nests

3.4.1. The Termite Colony

The small Najdian Termite, *Microtermes najdensis* [7,9,111,112] is shown in Figure 2.

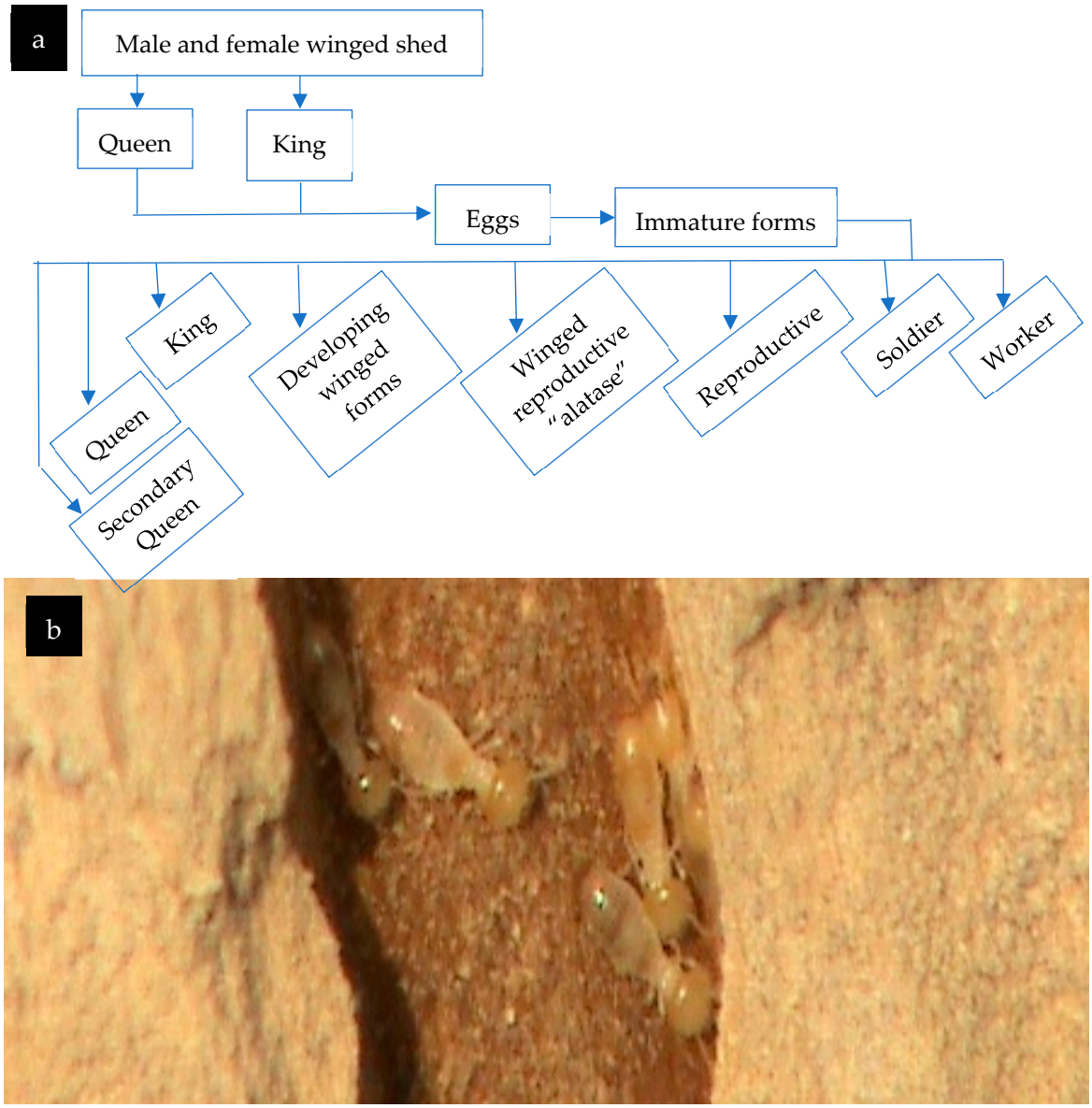

Figure 7. The studied the Najdian Termite, *Microtermes najdensis*: **(a)** their life cycle; **(b)** the workers within a living infected trunk of *Zizyphus spina christi*.

Male and female winged shed Queen King Eggs Immature forms Queen Secondary Queen King Developing winged forms Winged reproductive "alatase" Reproductive Soldier Worker

Preprints (www.preprints.org) | NOT PEER-REVIEWED | Posted: 22 September 2023 doi:10.20944/preprints202309.1492.v1

3.4.2. The Termite Nest Skeleton (TNS)

Forty widely distributed species were surveyed in Hada Al-Sham and were found to be infected by this insect. The most dominant infected plants by this pest were *Tamarix aphylla*, *Pithecellobium duce*, *Zizyphus spina christi*, *Leucaena leucocephala*, *Ficus infectoria*, and *Phoenix dactylifera*.

The infection aspects of *Zizyphus spina Christi*' s wood infected by the Najdian Termite, *Microtermes najdensis* are shown in Figure 8. It can be seen from Figure 8a that termite started to infect the sapwood, other than the heartwood of the infected log. This aspect is attributed to that heartwood is more enduring to the termites' infestation due to its high content of the organic extractives comparing to the sapwood. In addition, bark of the infected *Zizyphus* tree was swollen and peeled easily due to prominent of the tunnelS shielded by a ceiling made up of a thick layer of the mortar. In addition, huge number of entryways noticed at the southwest direction. This direction was not selected by termites fortuitously, but they allowed their nests to have better aeration and more efficient gas exchange achievement.

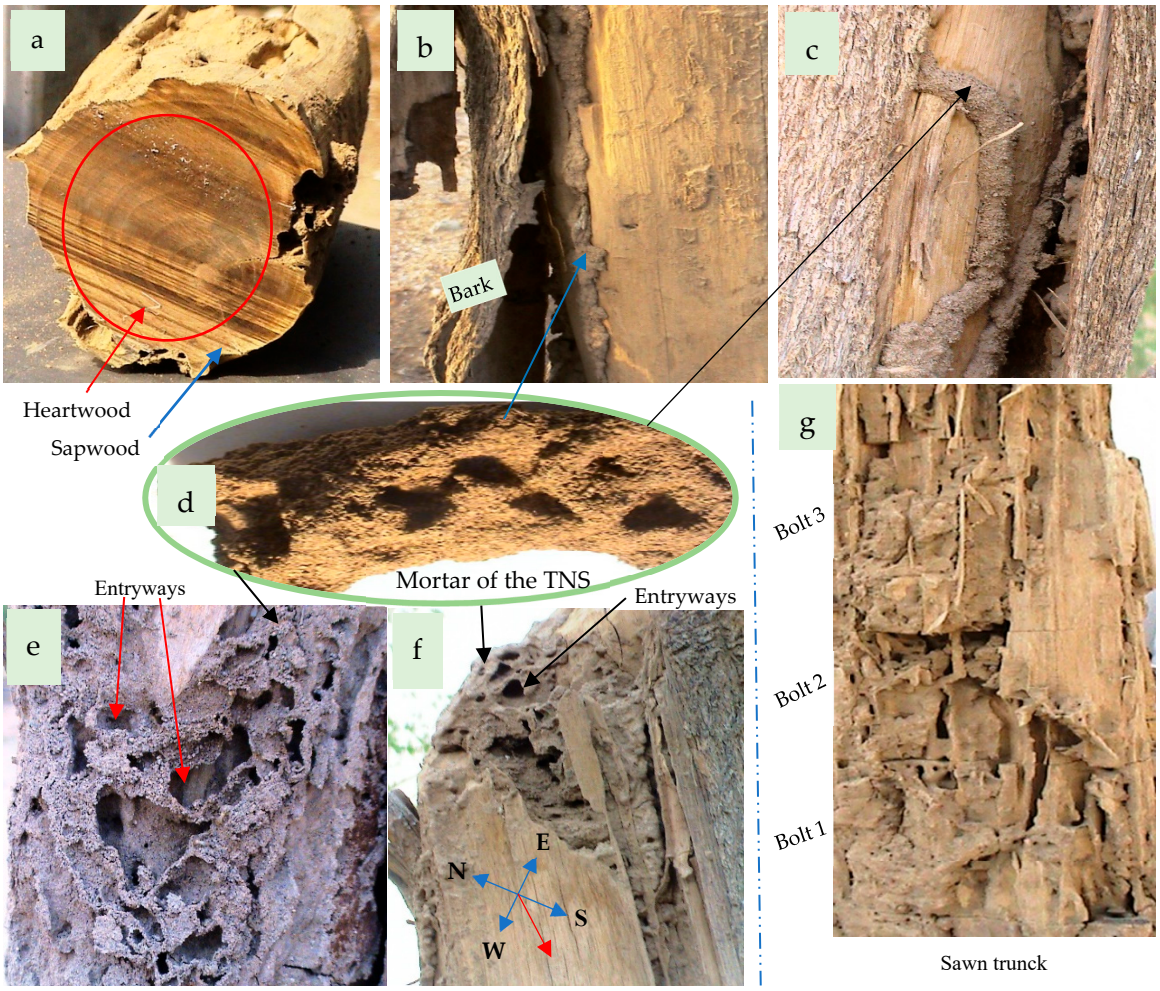

Figure 8. Optical images of the infection aspects of *Zizyphus spina Christi*' s wood infected by the Najdian Termite, *Microtermes najdensis*: (a) a fall crosscut woody log featured by its degraded sapwood, while its heartwood is still intact; (b) a still living infected trunk featured by its swollen peeled bark, (c) a tunnel shielded by a ceiling made up of a thick layer of the mortar; (d) mortar of the termite nest skeleton (TNS), e,f) entryways noticed at the southwest direction.

3.4.2.1. Mineral Matter (MM) of the TNS

I. Particle size (PS)

It can be seen from Figure 9 that the parent soils collected outside the termite nests just beneath each tree of the six species have highest fractions of the coarse particles [> 425μ] for both *Tamarix*

Preprints (www.preprints.org) | NOT PEER-REVIEWED | Posted: 22 September 2023 doi:10.20944/preprints202309.1492.v1

nilotica and *Zizyphus spina Christ*. On the other hand for the other four species sites, their major soil particles fractions are between 125-300 µ followed those higher than 425 µ

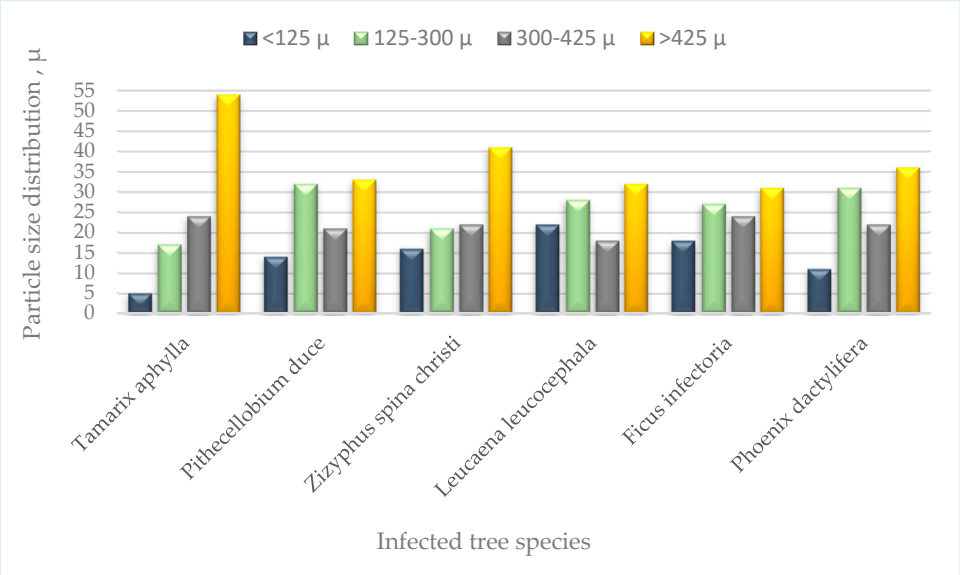

Figure 9. Particle size distribution (PSD) of the termite nest skeleton (TNS) occupied trunks of the six tree species.

II. Organic Matter Content (OMC) MiC of the TNS

The mineral content that was determined according to the related standard methods of the nest mortar ranged from 84.1 % for *Phoenix dactylifera* to 92.3 % for *Pithecellobium duce* (Figure 10). In addition, it can be seen that the minerals are considered as the most abundant constituent of the termite nest mortar. These results are in adaptance with those indicated by Ptáček et al. [47], and Rückamp et al. [66].

The OMC of the nest mortar was ranged from 7.7 % for *Pithecellobium duce* to 15.9 % for *Phoenix dactylifera* (Figure 10). There is no correlation relationship between the OMC and the lignin content of wood.

Preprints (www.preprints.org) | NOT PEER-REVIEWED | Posted: 22 September 2023 doi:10.20944/preprints202309.1492.v1

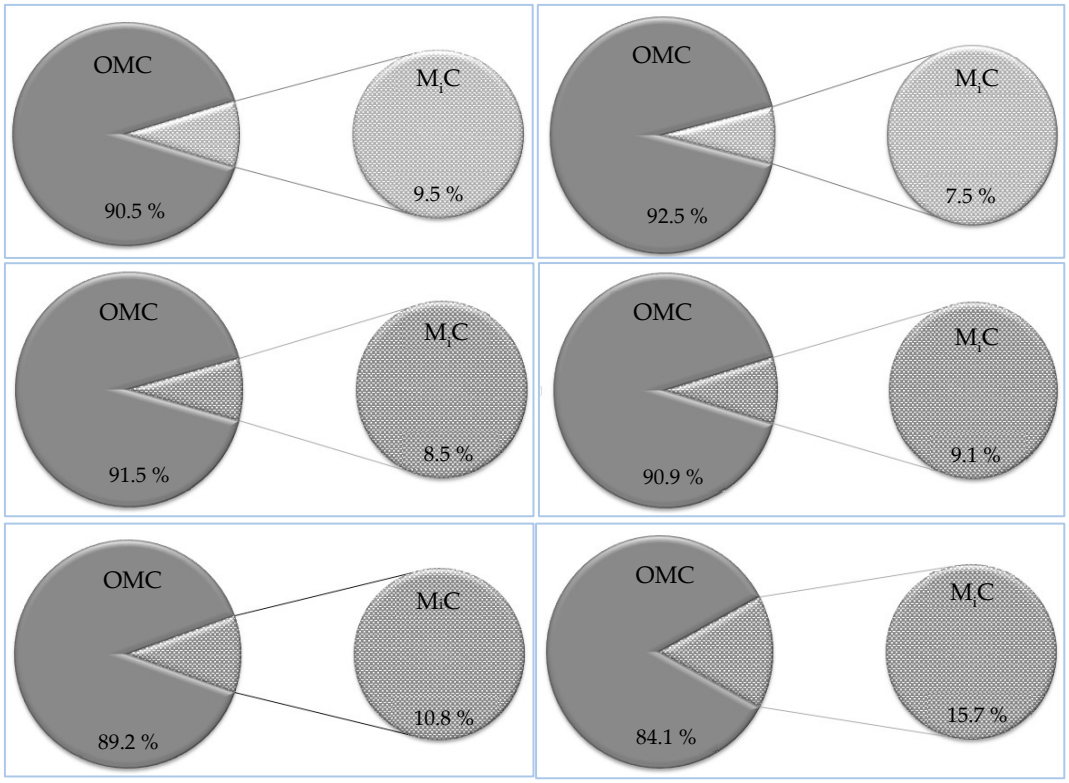

Figure 10. Organic matter content (OMC) and mineral content (MiC) of termite nest skeleton (TNS) occupied trunks of the six tree species: **(a)** Tamarix aphylla, **(b)** Pithecellobium duce, **(c)** Zizyphus spina Christi, **(d)** Leucaena leucocephala, **(e)** Ficus infectoria, and **(f)** Phoenix dactylifera.

III. Lignin content in the nest mortar

Lignin, the organic macromolecule constituting about 20-30 % of the secondary cell wall of wood. It is worth for mentioning that termites feeding on wood use the easily degradable cellulose components rather than lignin as carbon and energy source. Since lignin resists degradation by most termite species, it could be a prominent tracer of the organic matter incorporated into termite nests and released into nest surroundings [66].

It can be seen from Figure 11 the allocation of both organic matter content (OMC) and the Klason lignin content (KLC) from old nests (KLC-O) and recent nests (KLC-R) skeletons within the trunks of the six infected tree species, namely *Tamarix aphylla*, *Pithecellobium duce*, *Zizyphus spina Christi*, *Leucaena leucocephala*, *Ficus infectoria,* and *Phoenix dactylifera*.

Higher values of the lignin contents within the recent built nests can be revealed to that lignin content of the nests is detereorated as they increased in age.

Preprints (www.preprints.org) | NOT PEER-REVIEWED | Posted: 22 September 2023 doi:10.20944/preprints202309.1492.v1

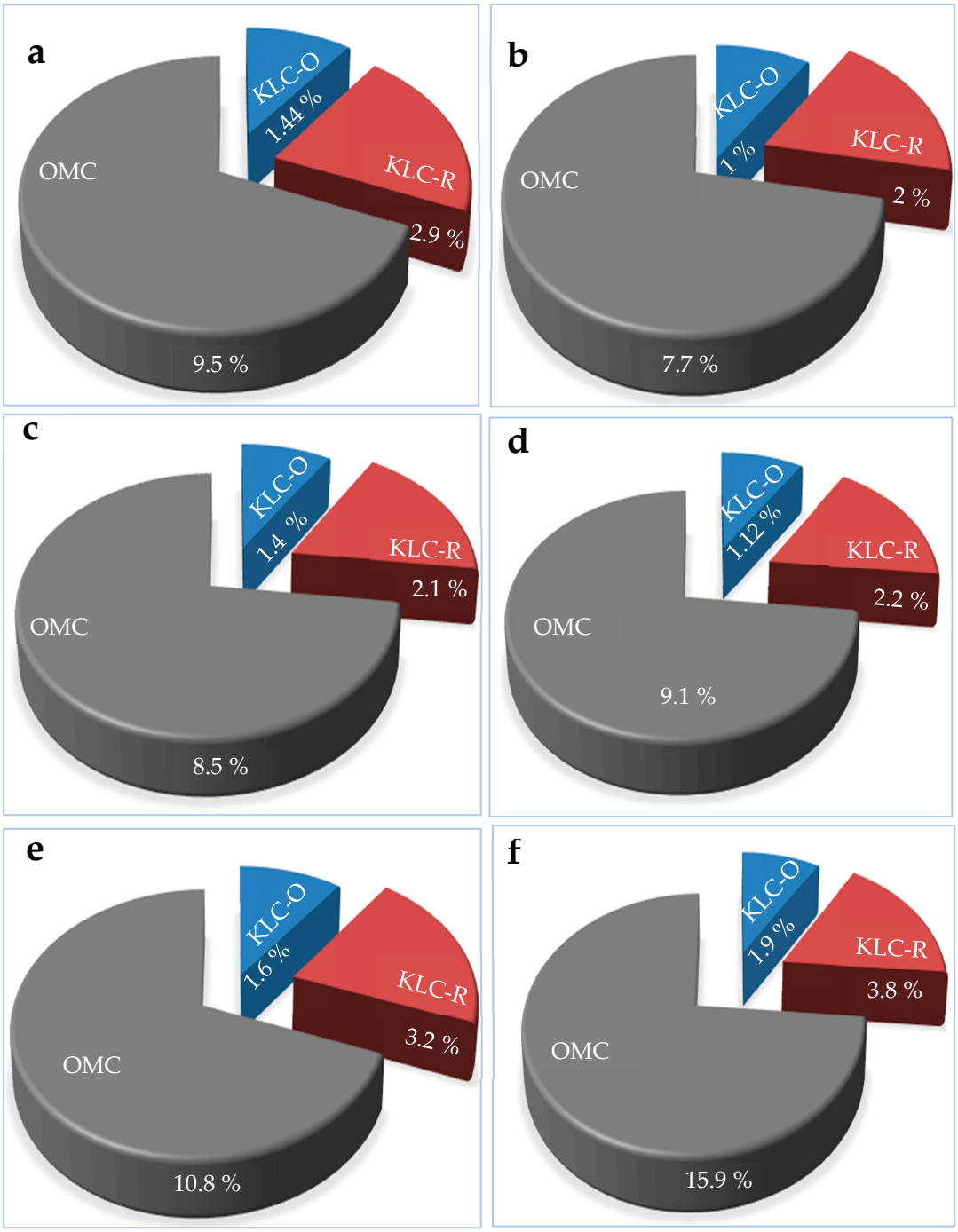

Figure 11. The allocation of organic matter content (OMC) and the Klason lignin content (KLC) from old nests (KLC-O) and recent nests (KLC-R) skeletons within the trunks of the six tree species: (a) *Tamarix aphylla*, (b) *Pithecellobium duce*, (c) *Zizyphus spina Christi*, (d) *Leucaena leucocephala*, (e) *Ficus infectoria*, and (f) *Phoenix dactylifera*.

Both, OMC and KLS contents were higher in termite nests than those of the reference soil (Table 3 and Figure 11). The KLC was even more enriched than OMC in the termite nest mortar. This is due to termites use lignin as the main organic binding agent in the nest mortar.

The relationship between the KLC of each of W_h and TNS

Preprints (www.preprints.org) | NOT PEER-REVIEWED | Posted: 22 September 2023 doi:10.20944/preprints202309.1492.v1

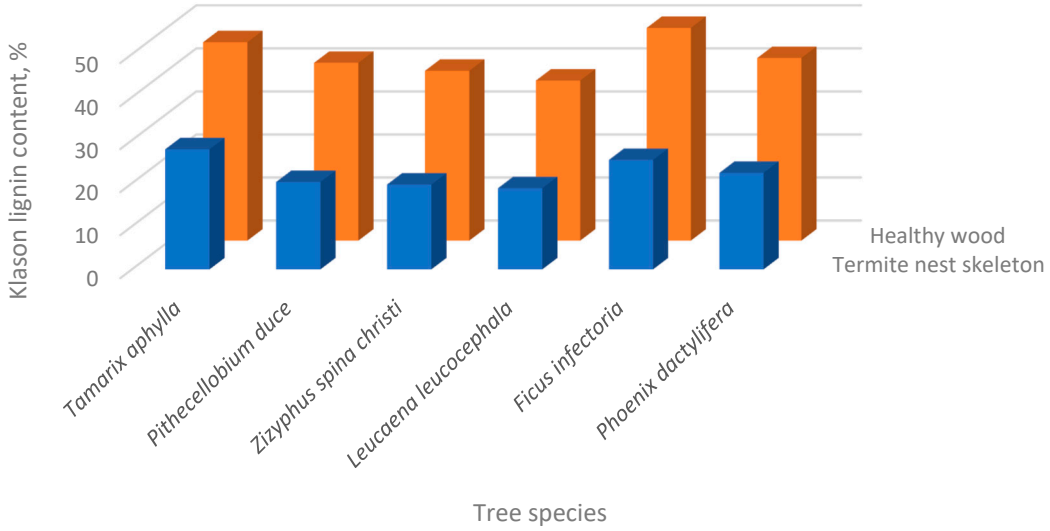

Figure 12. Klason lignin content (KLC) of the healthy wood (W_h) and the termite nest skeleton (TNS) occupied each of the six tree species.

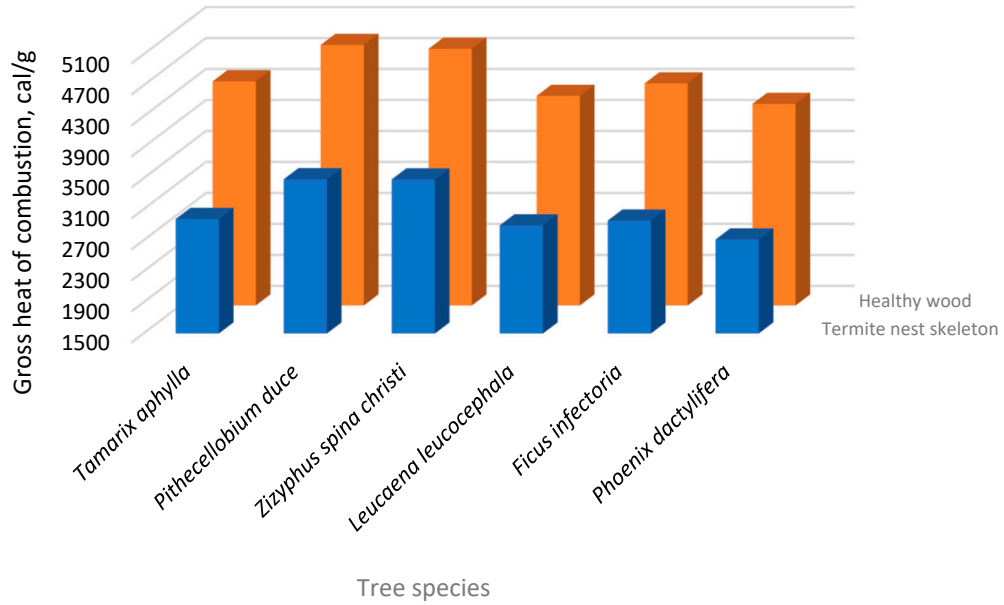

Figure 13. Gross heat of combustion (GHC) of the healthy wood (W_h) and the termite nest skeleton (TNS) occupied each of the six tree species.

3.5. Nanocelluloses Reinforcing the TNS

The nanometric-cellulosic materials (MCC, NCC) were surprised to be synthesized naturally by the act of hydrolyzing enzymes of the fungal communities and/or the termites' digestion detected within the termites' nest skeletons (TNS) within each of the six infected tree species.

The TNS' samples were examined spectroscopically by SEM technique in order to speculate their surface morphology and types of anatomical features as presented at Figure 14 (for the MCC's microparticles) and Figure 14 (for the NCC's nanoparticles [70,71].

3.5.1. Microcrystalline cellulose (MCC)

 doi:10.20944/preprints202309.1492.v1

Depending on Hindi [68,69], excess investigation of the six TNS specimens collected from the six tree species was achieved. In addition, SEM, FTIR, XRD examinations were performed to confirm presence of the MCC in the nest's mortar as a secondary binder agent.

The obtained data of the MCC material were presented at Figures 14, 16, and 17 for SEM, FTIR, and XRD, respectively. All the above-mentioned analyses tools confirmed that the micrometric particles detected were MCCs.

Concerning to the SEM micrographs shown in Figure 14, all the six subfigures (a-f) are presented in a micrometric scale ranged gradually from 50 µm (*Tamarix aphylla*, *Pithecellobium duce*, and *Leucaena leucocephala*), 100 µm (*Phoenix dactylifera*), 200 µm (*Zizyphus spina Christi*), and 400 µm for *Ficus infectoria*. This difference in magnification between the subfigures can be attributed to our trial to reach the best resolution. Moreover, we think that the SEM' dimensions for both MCC and NCC were less accurate to depend on comparing to the other tools (FTIR AND XRD). This difference in accuracy for the SEM's image dimensions is attributed to the crystal growth phenomenon discovered previously by Hindi [70,71] for NCC

Preprints (www.preprints.org) | NOT PEER-REVIEWED | Posted: 22 September 2023 doi:10.20944/preprints202309.1492.v1

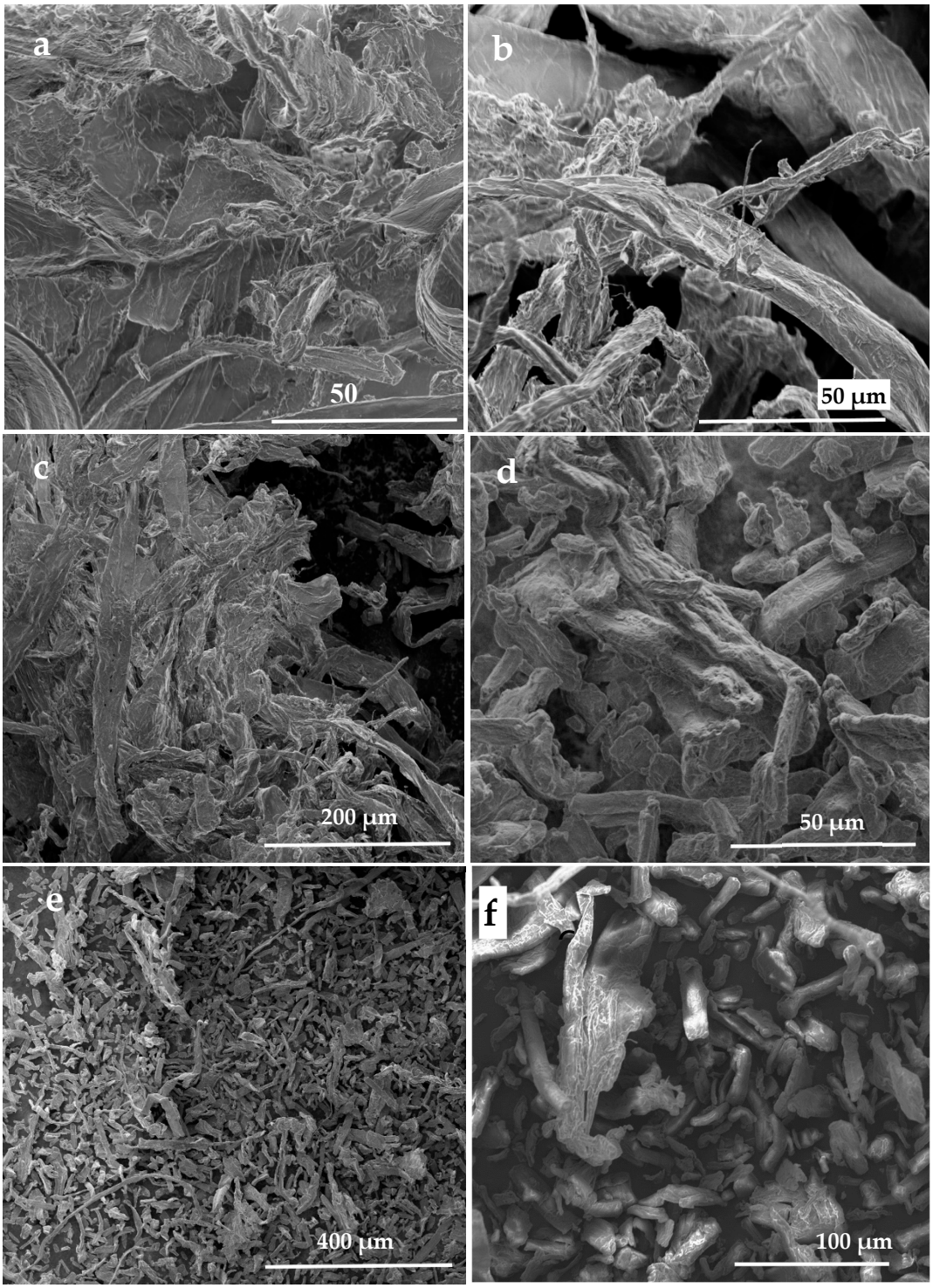

Figure 14. SEM micrographs of the microcrystalline cellulose (MCC) synthesized naturally by termites' enzymatic hydrolysis of cellulose as detected in the termit nest skeleton (TNS) within the six infected tree species: **(a)** Tamarix aphylla, **(b**) Pithecellobium duce, **(c)** Zizyphus spina Christi, **(d**) Leucaena leucocephala, **(e)** Ficus infectoria, and **(f)** Phoenix dactylifera.

3.5.2. Nanocrystalline Cellulose (NCC)

This difference in accuracy for the SEM's image dimensions is attributed to the crystal growth phenomenon discovered previously by Hindi [70,71] for NCC

It can be seen from Figure 15 that the scale bar of the six SEM's images for the NCCs ranged from 100 nm to 500 nm [68-76,113]. For first scond, these dimensions are greater than those legally accepted according to Hindi [68] who reported that nanocellulose must have at least one dimension

 doi:10.20944/preprints202309.1492.v1

less than 100 nanometers in size. Really, we found that the NCC's dimension always starting from about 5 nm, and after that the nanoparticle's dimension increases through a self process termed as grystal growth [70,71]. This crystal development process from nano- to micrometric size demonstrated the NCCs' aptitude for self-organization, or so-called self-assembly. It was discovered that after about 30 minutes of spreading a drop of the hydrolysis supernant onto the sample's stup of the SEM microscope, the NCCs spherulites were agglomerated into larger aggregates of colloidal state, which were then aligned straightly to form needle-shaped architectures.

The driving force for this crystal growth process can be limited to the following effects: a) electrostatic forces on the NCCs surfaces due to the grafted functional groups (protons, sulfate, and hydroxyl), b) the concentration gradient of the fungal communities' hydrolyzing enzymes and/or termite digestion, and c) the difference in surface tensions of solution, air, and glass. The net force produced at this interaction is thought to be the driving force behind the NCCs-crystal formation process. As a result, the needles were conceived to be created through electrostatic end-to-end attraction and subsequent self-welding of small NCC particles into larger ones [68,70-73]. However, it can be noticed from Figure 15 that there are a wide variation in particle size of the NCCs that confirms our theory of the NCC's crystal grows.

Moreover, since the presence of the nanocelluloses incorporated within the TNS' mortar was dicovered for the first time, it was expected that this phenomenon is one of the important reasons that strengthen the TNS that help them to endure different environment stresses.

Preprints (www.preprints.org) | NOT PEER-REVIEWED | Posted: 22 September 2023 doi:10.20944/preprints202309.1492.v1

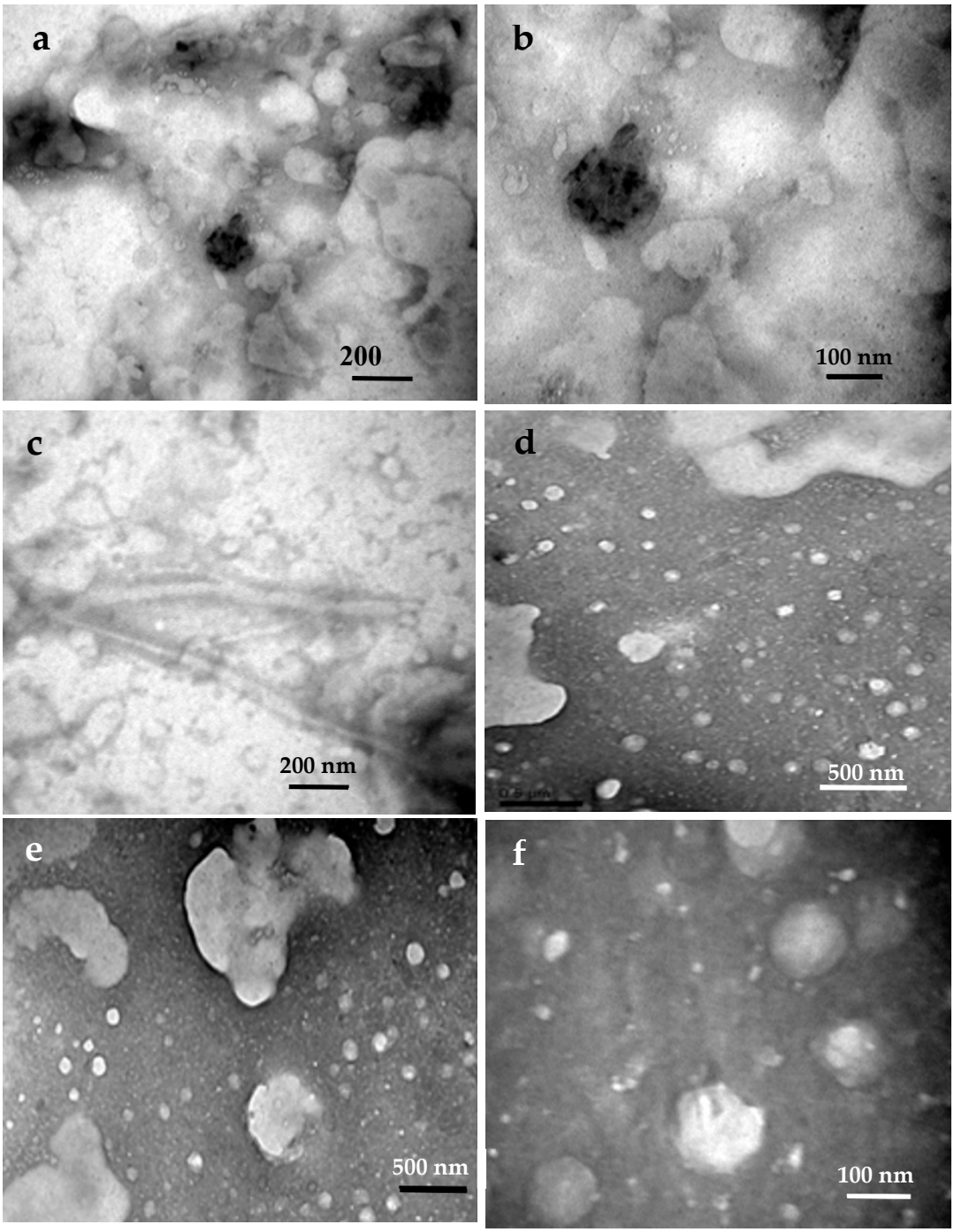

Figure 15. TEM micrographs of the nanocrystalline cellulose (NCC) synthesized naturally by termites' enzymatic hydrolysis of cellulose as detected in the termit nest skeleton (TNS) within the six infected tree species: **(a)** Tamarix aphylla, **(b)** Pithecellobium duce, **(c)** Zizyphus spina Christi, **(d)** Leucaena leucocephala, **(e)** Ficus infectoria, and **(f)** Phoenix dactylifera.

FTIR

The FTIR's spectrum of each alpha cellulose (C_α) and its nanocelluloses products, namely microcrystalline cellulose (MCC) and nanocrystalline cellulose (NCC) for the six tree species examined are presented at Figure 16. Moreover, the scientific illustration of arising these spectra were concluded at Table 5. showing the absorption bands of chemical (functional) groups featuring the examined cellulosic materials. Actually, all the samples exhibited two main absorbance regions detected (800–1800 cm^{-1} and 2800–3500 cm^{-1}). The FTIR spectra of all samples have shown sharp bands around the wavenumbers [70,71] presented at Table 5.

Preprints (www.preprints.org) | NOT PEER-REVIEWED | Posted: 22 September 2023 doi:10.20944/preprints202309.1492.v1

Table 5. The common absorption bands and their reasons for the alpha cellulose (C_α), microcrystalline cellulose (MCC), nanocrystalline cellulose (NCC) within the six infected tree species.

Wavenumber cm^{-1}	Reason of band appearance
1050	C–C ring stretching band and C–O–C glycosidic ether band.
1283	Scissoring motion of the CH_2-group.
1583	O-H bending of the absorbed water.
1658	C-O stretching vibration for the acetyl and ester linkages.
2850	C-H stretching.
3367	O-H stretching (axial vibration) intramolecular hydrogen bonds.

Based on the FTIR'S spectral data for C, MCC and NCC materials arisen from each of the six tree species (Figure 16), it can be confirmed that the principle constituent of the three cellulosic materials (C_α, MCC, NCC) were similar to each others which means that the nanometric particles detected (MCC and NCC) were nanocelluloses.

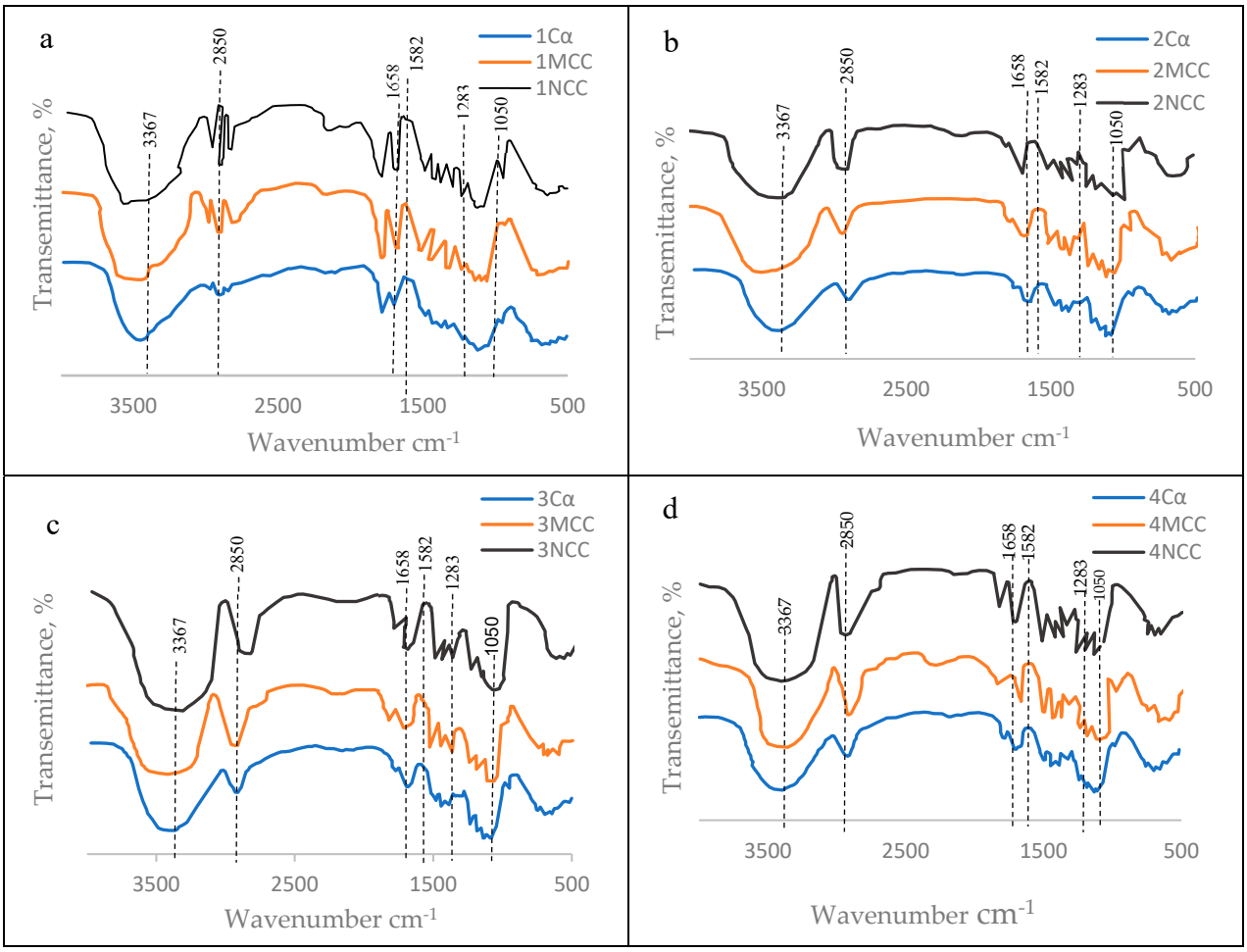

Preprints (www.preprints.org) | NOT PEER-REVIEWED | Posted: 22 September 2023 doi:10.20944/preprints202309.1492.v1

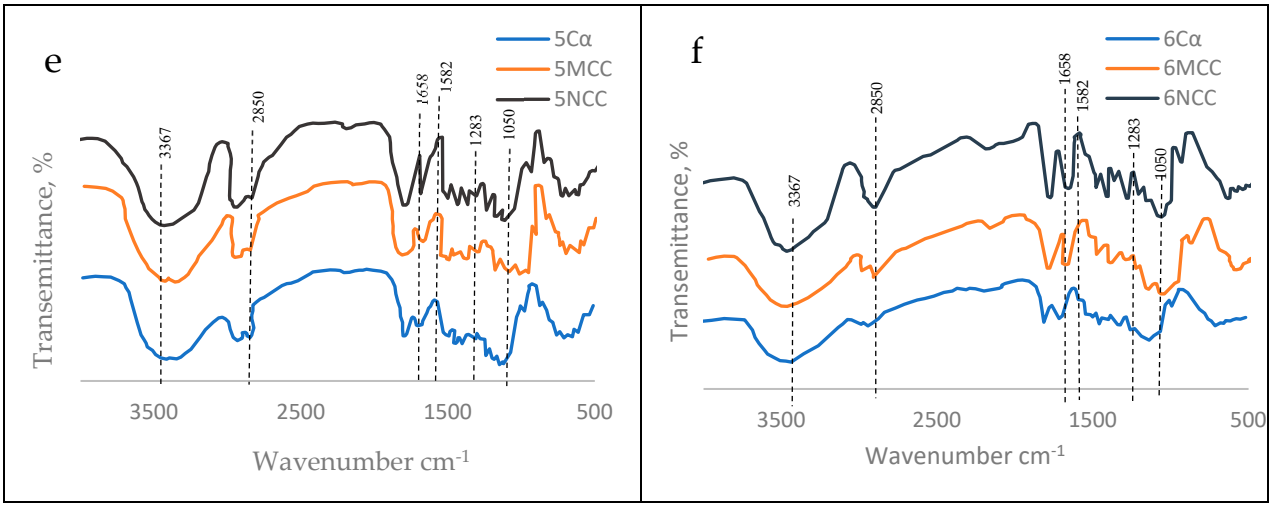

Figure 16. Fourier transform infrared (FTIR) spectra of the alpha cellulose (C_α), microcrystalline cellulose (MCC), nanocrystalline cellulose (NCC) within the six infected tree species: **(a)** *Tamarix aphylla*, **(b)** *Pithecellobium duce*, **(c)** *Zizyphus spina Christi*, **(d)** *Leucaena leucocephala*, **(e)** *Ficus infectoria*, and **(f)** *Phoenix dactylifera*.

The above mentioned explanation of the originality of both MCC and NCC from cellulose can be extended through studying their FTIR-bands (Figure 16) and reasons of their arrisen at certain wavenumbers (Table 5) as indicated by Hindi [69-71].

XRD

As clear in Figure 17 for the crystallographic findings, the crystallinity index was increased from crude wood passing through alpha cellulose, MCC and, finally ended by the NCC. This finding, also, confirms the presence of the nanocellulose in the six mortar blends as a result of enzymatic hydrolysis occuring by termits and/or fungi during their feeding and constructing their nests.

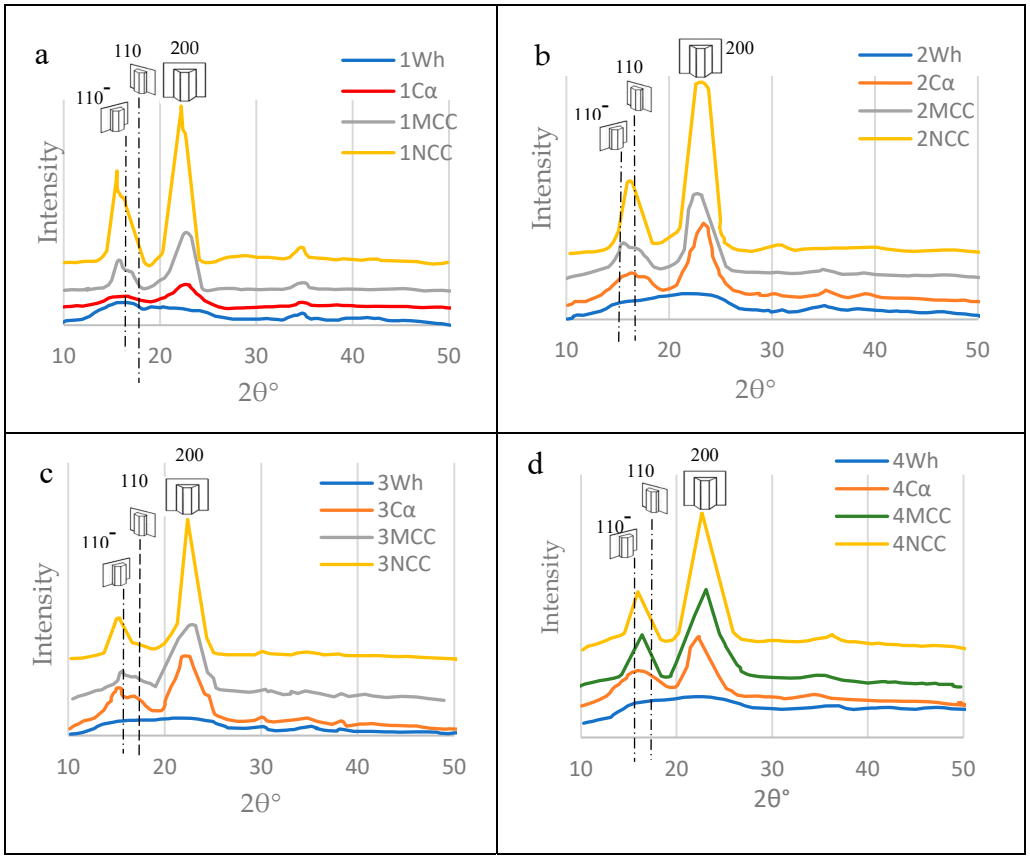

200

Preprints (www.preprints.org) | NOT PEER-REVIEWED | Posted: 22 September 2023 doi:10.20944/preprints202309.1492.v1

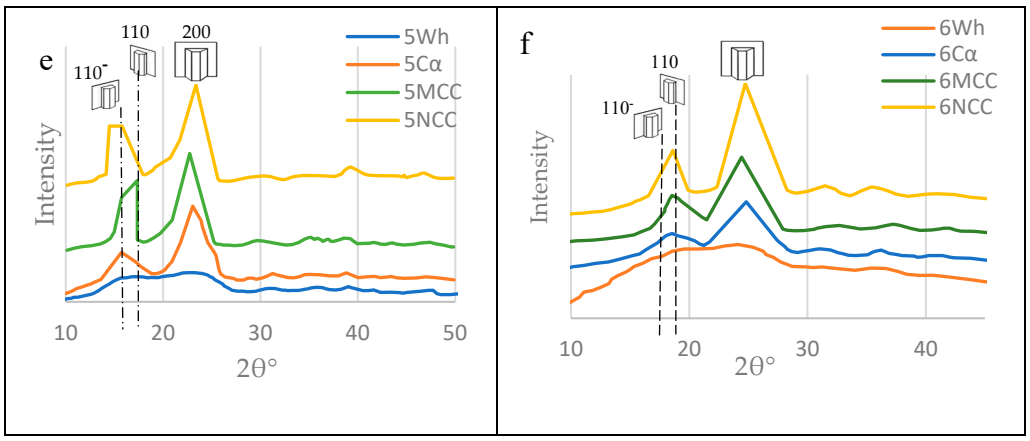

Figure 17. X-ray Diffractogram (XRD) of the healthy wood (W_h), alpha cellulose (C_α), microcrystalline cellulose (MCC), nanocrystalline cellulose (NCC) within the six infected tree species: **(a)** *Tamarix aphylla*, **(b)** *Pithecellobium duce*, **(c)** *Zizyphus spina Christi*, **(d)** *Leucaena leucocephala*, **(e)** *Ficus infectoria*, and **(f)** *Phoenix dactylifera*.

3.6. Mechanical Properties of the TNS as Affected by the Polymeric Blend

3.6.1. Stress–strain relationship of the TNS

The resulted histograms presented at Table 6, Figures 18 and 19 revealed that the ultimate compressive stresses (UCS) of the TNS constructed in the six infected tree species were differed significanly among species [95,114].

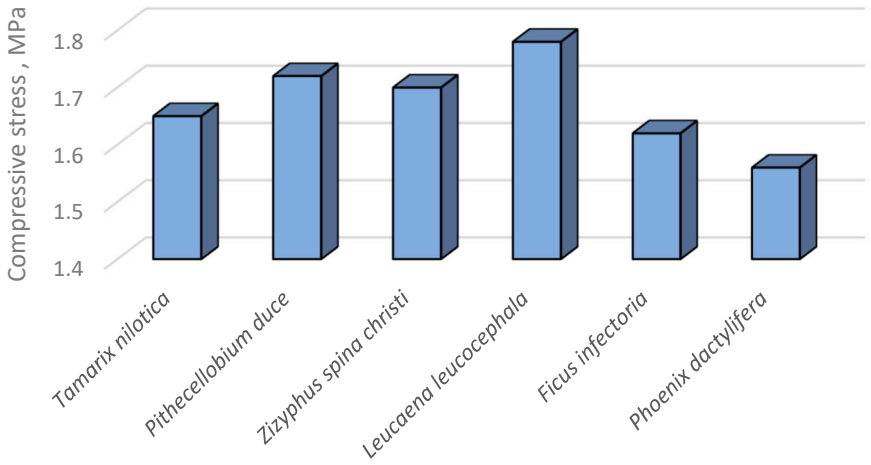

Figure 18. Ultimate compressive stress (UCS) of the termite nest skeleton (TNS) constructed in the six infected tree species.

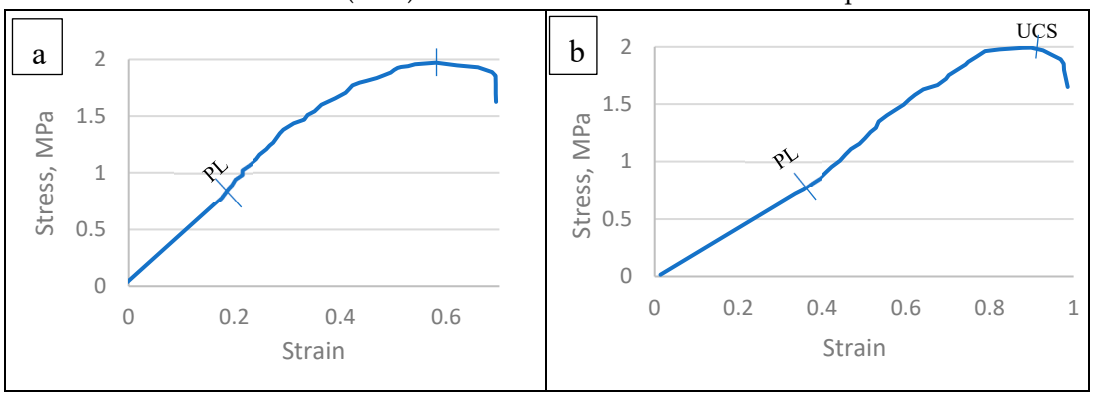

UCS

Preprints (www.preprints.org) | NOT PEER-REVIEWED | Posted: 22 September 2023 doi:10.20944/preprints202309.1492.v1

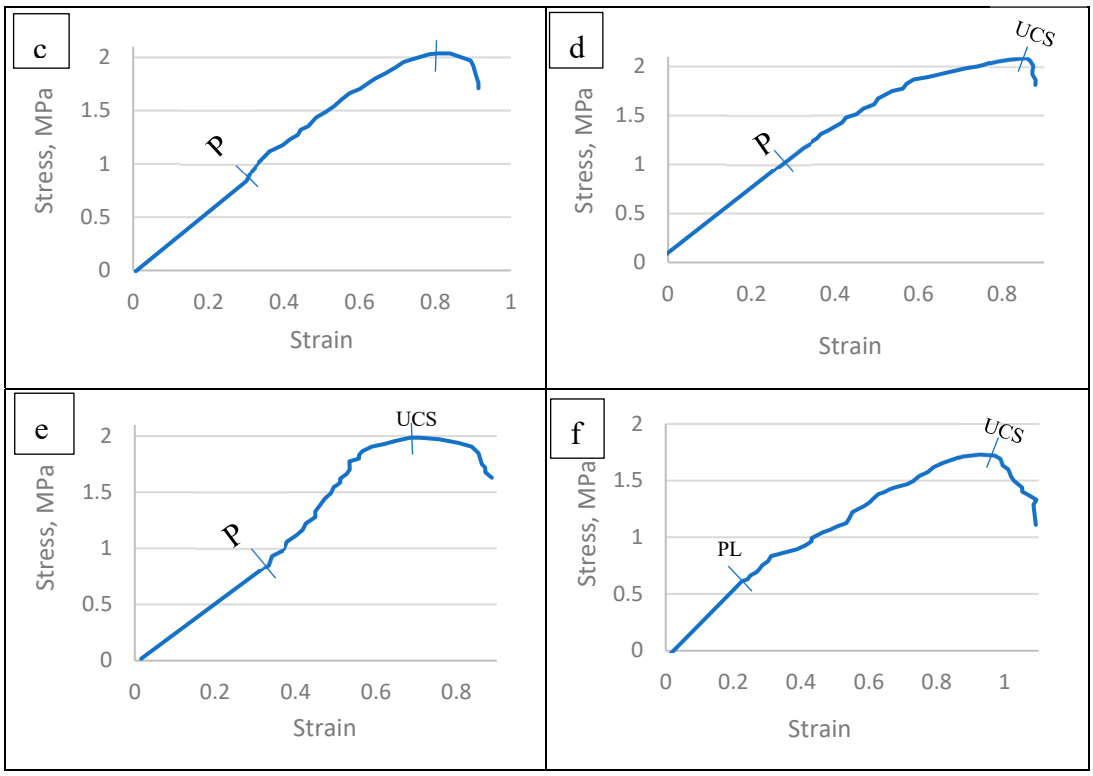

Figure 19. Stress–strain graphs of the termite nest skeleton (TNS) constructed in the six infected tree specie: **(a)** *Tamarix aphylla*, **(b)** *Pithecellobium duce*, **(c)** *Zizyphus spina Christi*, **(d)** *Leucaena leucocephala*, **(e)** *Ficus infectoria*, and **(f)** *Phoenix dactylifera* showing proportionality limit (PL) and ultimate compressive stress (UCS).

The mean values of proportionality limit (PL) and ultimate compressive stress (UCS) were presented at Table 6 and Figure 19. The PL values was found to be ranged between 0.814 MPa-1.116 MPa for *Pithecellobium duce* and *Leucaena leucocephala*, respectively. Moreover, the UCS the six infected tree species differed from 1.733 MPa up to 2.092 MPa for *Phoenix dactylifera* and *Leucaena leucocephala*, respectively. These differences in PL and UCS of the TNS' of the infected specimens collected from the six species may be attributed to their differences in densities and the chemical properties of the parent materials constituting the TNS' backbone.

Table 6. Proportionality limit (PL) and ultimate compressive stress (UCS) of the six infected tree species.

Species	Stress Type	Stress MPa	Strain
Tamarix aphylla	PL	0.865	0.188
	UCS	1.973	0.58
Pithecellobium duce	PL	0.814	0.375
	UCS	1.992	0.878
Zizyphus spina christi	PL	0.84	0.301
	UCS	2.037	0.805
Leucaena leucocephala	PL	1.116	0.305
	UCS	2.092	0.858
Ficus infectoria	PL	0.936	0.339
	UCS	1.987	0.685
Phoenix dactylifera	PL	0.664	0.251
	UCS	1.733	0.927

Each value is an average of 3 samples.

The MoE of the six infected tree species were presented at Figure 20.

Preprints (www.preprints.org) | NOT PEER-REVIEWED | Posted: 22 September 2023 doi:10.20944/preprints202309.1492.v1

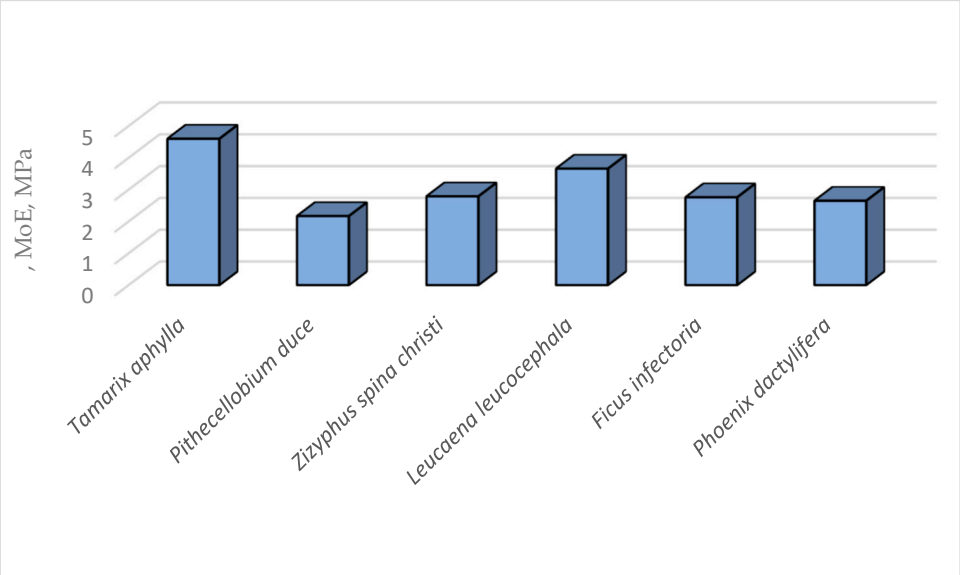

Figure 20. Modulus of Elasticity (MoE) of the termite nest skeleton (TNS) constructed naturally within the six infected tree species.

4. Conclusions and Future Perspectives

The composition and quality of the tunnels' mortar made by the Najdian Termite, *Microtermes najdensis* were extensively studied in the present investigation. The most by this pest. Climate, soil, healthy wood (Wh) as well as the termite nest skeleton (TNS) engraved within the prevalent infected timber trees were the four components of the termite system that were investigated physically, chemically and spectroscopically. The entryways of the termite nests were noticed to be located at the southwest direction for all the infected that promotes better ventilation. The internal temperature of the nests was recorded to be milder than the outer temperature in hot days and vice versa. This finding reflects that termites prefer hotter atmospheres than the colder circumstances. Lignin was proved to be the prominent binder for the mortar beside microcrystalline cellulose and nanocrystalline cellulose as discovered for the first time in the termite nest mortar. The reasonable calorific value of the infected wood open the door for practical utilization of such materials to be used as renewable energy resources instead of disposal them without economic benefits. These findings can help us for interpreting termite nests' durability to different environmental stresses. Biomimicry of the termites' nest construction can lead to modify the current construction's designs to be greener and ecofriendly.

Patents: Hindi, S.S.; Abouhassan, R.A. 2018. Method for making nanoocrystalline cellulose. US Patent, issue no. 10144786B2, issue date: 4 December 2018; Hindi, S.S. A method for converting micro- to nanocrystalline cellulose. US Patent, issue no. 10808045, issue date: 20 October 2020; Hindi, S.S. Nanocrystalline cellulose. U.S. patent no. 11161918, issue date: 11 February 2021; Hindi, S.S. Method for recovery of cellulosic material from waste lingocellulosic material. US Patent, issue no. 11136715, issue date: 10 May 2021; Hindi, S.S. A method for isolating alpha cellulose from lignocellulosic materials. U.S. patent, issue number 11078624, issue date: 03 August 2021; Hindi, S.S. Sulfate-grafted nanocrystalline cellulose. US Patent, issue no. 11242411, issue date: 8 February 2022; Hindi, S.S. Urchin-shaped nanocrystalline material. US Patent, issue no. 112424, issue date: 8 February 2022; Hindi, S.S. Method for separating lignin from lignocellulosic material. US Patent, issue no. 11, 306, 434B2, issue date: 18 April 2022.

Supplementary Materials: The following supporting information can be downloaded at: https://www.mdpi.com/article/10.3390/polym15102254/s1, Figure S1: Schematic representation of the procedure used for preparation of the experimental samples: a) healthy wood (W_h), and b) Termite nest skeleton (TNS) of the six tree species; Figure S2: Technical procedures, machinery and/or glassware used for characterization of the each of the healthy wood (W_h) and/or termite nest skeleton

(TNS): a) Soxhlet apparatus for extracting total extractives content (TEC) and alcohol benzene extractives (ABE), b) Refluxed Pyrex apparatus for chemical separation of Klason lignin content (KLC), c) Vacuum pump-assisted water-saturation of the W_h, d) Electric muffle furnace used for determination of ash content of W_h, and e) Porcelain crucibles containing W_h samples to be ashed within the muffle furnace; Figure S3: Gross heat of combustion determination (GHC): a) Parts of the oxygen bomb calorimeter used for measuring GHC of the healthy wood and the termite nest skeletons (TNS), and b) Typical temperature rising curve of a woody sample.

Author Contributions: Supervision, conceptualization, and methodology, S.S.H.; editing and revising, S.A.; drawing curves and software, N.A.A.; software and assistance with writing—original draft preparation, K.A.A.

Funding: This work was funded by the Deanship of Scientific Research [DSR], KAU, Jeddah under grant no. G: 85/155 /1434

Institutional Review Board Statement: Not applicable

Data Availability Statement: Not applicable.

Acknowledgments: The authors are deeply thankful to the DSR, KAU, Jeddah for funding this research work. Moreover, Deep thanks to Rakan A. Alanazi for his scientific assistance all over this investigation.

Conflicts of Interest: The authors declare no conflict of interest.

Nomenclature

Symbol	Definition	Symbol	Definition
ABE	Alcohol-benzene extractives	OC	Organic carbon
AC	Ash content	OMC	Organic matter content
ASTM	American Society for Testing and Materials	PL	Proportionality Limit
FID	Flame-ionization detection	PSD	Particle size distribution
GC/MS	Gas Chromatography coupled with mass spectrophotometer	sccm	Standard cubic centimeters per minute
HC	Holocelluloses	SEC	Soil Electrical Conductivity
KLC	Klason lignin content	SG	Specific gravity
LoI	loss on ignition	TEC	Total extractive content
M_iC	Mineral contents	UCS	Ultimate compressive stress
MoE	Modulus of Elasticity	UCD	Ultrafine cellulosic Derivatives
M_oC	Moisture content		

References

1. Gay, F.J.A world review of introduced species of termites. C.S.I.R.0. Melbourne, Bull. No. 286, **1967**, 88.
2. Li, H.; Greening, C. Termite-engineered microbial communities of termite nest structures: a new dimension to the extended phenotype. *FEMS Microbiol. Rev*. **2022**, 46, fuac034.
3. Badawi, A.; Al-Kady, H.; Faragalla, A.A. Some factors affecting the distribution and abundance of Termites in Saudi Arabia. *Anz. Schadlingskde., Pflanzenschutz, Umweltschutz*. **1986**, 59, 17–19.
4. Sharaf, M.R.; Husain, M.; Rasool, K.G.; Tufail. M.; Aldawood, A.S. Taxonomy and distribution of termite fauna (Isoptera) in Riyadh Province, the Kingdom of Saudi Arabia, with an updated list of termite species on the Arabian Peninsula. *Saudi J Biol Sci*. **2021** 28, 6795–6802.
5. Reginaldo, C.; Dianese, E.C. The urban termite fauna of Brasilia, Brazil (Isoptera). *Sociobiol*. **2001**, 38, 323–326.
6. Nutting, W.L.; Jones, S.C. Methods for studying the ecology of subterranean termites. *Sociobiol*. **1990**, 17, 167–189
7. Al-Ghamdi, K.M., Aseri, A.A. and Mayhoub, J.A. Field study on tunnel shapes of the small Najdian Termite, *Microtermes najdensis* (Isoptera: Macrotermetidae) and the percentage of infestation in its host plants in Makkah Al., Mokaramah Province. MSc thesis, Department of Biological Sciences, Faculty of Science, King Abdulaziz University, Jeddah, Saudi Arabia. **2009**.
8. Faragalla, A.A.; Mohamed H.; Al Qhtani, M.H. The Urban termite fauna (Isoptera) of Jeddah City, Western Saudi Arabia. *Life Sci. J*. **2013**, 10, 1695–1701.

9. Johnson, R.A.; Wood, T.G. Termites of the arid zones of Africa and the Arabian Peninsula. *Sociobiol*. **1980**, 5: 279–93.
10. Nasr, H.; Al-Hadiy, F.; Halawani, M.; Al-Ghamdi, M. The use of soil pesticides in the control of termites in certain vegetable crops, Annual Technical Report, Agricultural Research Center, Western Region, Saudi Arabia. **1980**, 46–47.
11. Su, N.Y.; Scheffrahn, R.H. A review of subterranean termite control practices and prospects for integrated pest management programmes. *Integr. Pest Manag. Rev.* **1998**, 3, 1–13.
12. Koehler, P.G.; Short, D.E.; Kern, W.H. Pests in and around the Florida home. University of Florida Cooperative Extension Service, IFAS No SP 134. Gainesville FL. **1998**.
13. Jost, C. Nest-structure: termites. 2021. In: Encyclopedia of social insects, Starr, C.K. ed. Cham, Switzerland, Springer. **2020**, 651-660.
14. Turner, J.S.; Soar, R.C. Beyond biomimicry: What termites can tell us about realizing the living building? Proceedings of 1st International Conference on Industrialized, Intelligent Construction. 01 January **2008.**
15. Hindi, S.S.; Abohassan, R.A. Cellulosic microfibril and its embedding matrix within plant cell wall. *Int. J. Innov. Res. Sci. Eng. Technol.* **2016**, 5, 2727–2734.
16. Matthews, J.F.; Himmel, M.E.; Brady, J.W. Simulations of the structure of cellulose. Computational modeling in lignocellulosic biofuel production: ACS Symposium Series. **2010**, 1052, 17–53.
17. Brett, C.T. Cellulose microfibrils in plants: biosynthesis, deposition, and integration into the cell wall. *Int. Rev. Cytol.* **2000**, 199, 161–199.
18. Somerville, C. Cellulose synthesis in higher plants. *Annu. Rev. Cell Dev. Biol*. **2006**, 22, 53–78.
19. Klemm, D., Heublein, B., Fink, H.P. and Bohn, A. Cellulose: fascinating biopolymer and sustainable raw material. Angew. Chem., Int. Ed. Engl. **2005**, 44, 3358–3393.
20. Zabel, R.A, Morrell, J.J. Wood microbiology: Decay and its prevention. Academic Press, New York. **1992**.
21. Varma, A.; Kolli, B.K.; Paul, J.; Saxena, S.; König, H. Lignocellulose degradation by microorganisms from termite hills and termite guts: A survey on the present state of art. *FEMS Microbiol. Rev*. 1**994**, 15, 9–28.
22. Oppert, C.; Klingeman, W.E.; Willis, J.D.; Oppert, B.; Jurat-fuentes, J.L. Prospecting for cellulolytic activity in insect digestive fluids. *Comp. Biochem. Physiol. B, Biochem. Mol. Biol*. **2010**, 155, 145–54.
23. Scheller, H.V.; Ulvskov, P. Hemicelluloses. *Annu. Rev. Plant Biol*. **2010**, 61, 263–289.
24. Keegstra, K.; Talmadge, K.W., Bauer, W.D., Albersheim, P. The structure of plant cell walls: III. A model of the walls of suspension-cultured sycamore cells based on the interconnections of the macromolecular components. *Plant Physiol.* 1973, 51, 188–197.
25. Eriksson, K. EL. Concluding remarks: Where do we stand and where are we going?: Lignin biodegradation and practical utilization. *J. Biotechnol*. **1993**, 30, 149–58.
26. Wood, T.G. and Sands, W.A. The role of termites in ecosystems. In: Brain, M.V., Ed., Production ecology of ants and termites. Cambridge, Cambridge University Press. **1978**, 245–292.
27. Faragalla, A.A. Termite problems in Saudi Arabian ecosystems. Sociobiology. **1983**, 8,119–125.
28. Faragalla, A.A. Impact of agro desert on a desert ecosystem. *J. Arid Environ*. **1988**, 15:99–102.
29. Ulyshen, M. D. Wood decomposition as influenced by invertebrates. *Biol. Rev*. **2014**, 91, 70–85.
30. Collins, N.M. Consumption of wood by artificially isolated colonies of fungus-growing termite *Mastotermes bellicosus*. *Entomol. Exp. Appl*. **1981**, 29, 313–320.
31. Darlington, J.P.E.C. Termite nests in a mound field at Oleserewa, Kenya (Isoptera: Macrotermitinae). Sociobiol. **2000**, 35, 25–34.
32. Krishna, K. Order Isóptera: Termites. In: Borror, D.J; Triplehorn C.A.; Johnson, N.F (Eds). An introduction to the study of insects (6th Edition). Saunders College Publishing, Philadelphia, PA. **1989**, 234–241.
33. Grace, K.J. Response of eastern and Formosan subterranean termites (Isoptera: Rhinotermitidae) to borate dust and soil treatments. *J. Econ. Entomol*. **1991**, 84, 1753–1757.
34. Eggleton, P.; Bignell, D.E. Monitoring the response of tropical insects to changes in the environment: Troubles with termites. In: Harrington, R. and Stork. (Eds). Insects in a changing environment. London. Heademic Press. **1995**, 473–497.
35. Faragalla, A.A.; AL-Ghamdi, K.M.S. Monitoring field populations of the harvester termite Anacanthotermes ochraceous (Burmeister) in two locations in western Saudi Arabia. *Sociobiol*. **1999**, 34, 419–427.
36. Nash, M.; Anderson, J.P.; Whitford, W.G. Spatial and temporal variability in foraging intensities of subterranean termites in decertified and relatively intact Chihuahua desert ecosystem. *App. Soil Ecol*. 1999, 12, 149–157.
37. Su, N.Y; La Fage, J.P. Forager populations and caste composition of colonies of the Formosan subterranean termite (Isoptera: Rhinotermitidae) restricted to cypress trees in the clacasteus river, Lake Charies, Louisiana. *Sociobiol*. **1999**, 33, 185–193.
38. Whitford, W.G. Effects of habitat characteristics on the abundance and activity of subterranean termites in arid Southeastern New Mexico (Isoptera). *Sociobiol*. **1999**, 34, 493–504.

39. Stewart, A.Termite foraging interaction with a protective barrier system. A PhD. Thesis, Sustainable Mineral Institute, the University of Queensland, Australia. **2009**, 156.
40. Miller, D.M., 2010. Subterranean termite's biology and behavior. Virginia Cooperative Extension.
41. Suiter, D.R.; Jones, S.C.; Forschler, B.T. Biology of subterranean termites in the Eastern United States. Bulletin 1209. The Ohio State University. **2010**.
42. Duryea, M.L. Landscape Mulches. Will subterranean termites consume them? University of Florida IFAS Extension Publication. **2011**.
43. Arshad, M.A. Physical and chemical properties of termite mounds of two species of Microcerotermes (Isoptera: Termitidae) and the surrounding soils of the semi-arid Savanna of Kenya. *Soil Sci*. **1981**,132, 161–174.
44. Al-Ghamdi, K.M.; Faragalla, A.A. Field Study on gallery shapes of the harvester termite Anacanthotermes ochraceous (Burmeistser) (Isoptera: Hodotermitidae) from different localities in Western Saudi Arabia. *Annals of Agric. Sci. Moshtohor*. **1998**, 36, 1135–1144.
45. Chouvenc, T.; Su, N.-Y. When subterranean termite challenge the rules for fungal epizootic. *PLoSOne*. 2012, 7, e 34484.
46. Donovan, S. E.; Jones, D.T.; Sands, W.A.; Eggleton, P. Morphological phylogenetics of termites (Isoptera). *Biol. J. Linn. Soc*. **2000**, 70, 467–513.
47. Ptáček, P.; Brandštetr, J.; Šoukal, F.; Opravil, T. Investigation of subterranean termites nest material composition, structure and properties. Intech, Chapter 20. **2013**, 519–549.
48. Mattéotti Ch., Bauwens J, Brasseur C, et al. Identification and characterization of a new xylanase from Gram-positive bacteria isolated from termite gut [*Reticulitermes santonensis*]. *Protein Expr. Purif*. **2012**, 83, 117–127.
49. Slaytor, M. Cellulose digestion in termites and cockroaches: What role do symbionts play? *Comp. Biochem. Physiol. B, Comp. Biochem*. **1992**, 103, 775–84.
50. Buxton, R.D. Termites and the turnover of dead wood in an arid tropical environment. *Oecologia*. **1981**, 51, 379–84.
51. Grassé, P.; Noirot, P.C. Le meule des termites champignonnistes et sa signification symbiotique. *Ann. sci. nat., Zool. biol. anim*. **1958**, 11, 113–28.
52. Hyodo, F.; Inoue, T.; Azuma, J.; Tayasu, I.; Abe, I.T. Role of the mutualistic fungus in lignin degradation in the fungus-growing termite *Macrotermes gilvus* (Isoptera: Macrotermitinae). *Soil Biol. Biochem*. **2000**, 32, 653–8.
53. Crawford, D.L.; Crawford, R.L. Microbial degradation of lignocellulose: the lignin component. *Appl. Environ. Microbiol*. **1976**, 31, 714–717.
54. Crawford, D.L.; Crawford, R.L.; Pometto A. L. Preparation of specifically labeled 14C-(lignin) – and 14C–(cellulose) –lignocelluloses and their decomposition by the microflora of soil. *Appl. Environ. Microbiol*. **1977**, 33, 1247–1251.
55. Crawford, D.L. Lignocellulose decomposition by selected Streptomyces strains. *Appl. Environ. Microbiol*. **1978**, 35, 1041–1045.
56. Crawford, D.L. Microbial conversions of lignin to useful chemicals using a lignin–degrading Streptomyces. *Biotechnol. Bioeng. Symp*. **1981**, 11, 275–291.
57. Crawford, D.L., Barder, M.J.; Pometto, A.L.; R. Crawford, R.L. Chemistry of softwood lignin degradation by a Streptomyces. Arch. *Microbiol*. **1982**, 131, 140–145.
58. Crawford, D.L., Pometto A.L.; Crawford, R.L. Lignin degradation by *Streptomyces viridosporus*: isolation and characterization of a new polymeric lignin degradation intermediate. *Appl. Environ. Microbiol*. **1983**, 45, 898–904
59. Crawford, D.L.; Pettey, T.M.; Thede, B.M.; Deobald, L.A. Genetic manipulation of ligninolytic Streptomyces and generation of improved lignin to chemical bioconversion strains. *Biotechnol. Bioeng. Symp*. **1984**, 14, 241–256.
60. Crawford, D.L. The role of actinomycetes in the decomposition of lignocellulose. *FEMS Symp*. **1986**, 34, 715–728.
61. Kirk, T.K., and Farrell, R.L. Enzymatic combustion: the microbial degradation of lignin. *Annu. Rev. Microbiol*.**1987**, 41, 465–505.
62. Haug, R.T. The Practical Handbook of Compost Engineering; Lewis Publishers: Boca Raton, FL. **1993**.
63. Badawi, A.I.; Faragalla, A.A.; Dabbour. A.I. The role of termites in changing certain chemical characteristics of the soil. *Sociobiol*. **1982**, 7, 135–144.
64. Sabine, G. Soil modification by the harvester termite *Hodotermes mossambicus* (Isoptera: Hodotermitidae) in a semi-arid savanna glass land of Namibia. *Sociobiol*. **2001**, 37, 757–767.
65. Tuomela, M, Vikman, M, Hatakka, A, & Itävaara, M. Biodegradation of lignin in a compost environment: a review. *Bioresour. Technol*. **2000**, 72, 169–83.
66. Rasse, D.P.; Dignac, M.-F.; Bahri, H.; Rumpel, C.; Mariotti, A.; Chenu, C.. Lignin turnover in an agricultural field: From plant residues to soil-protected fractions. *Eur. J. Soil Sci*. **2006**, 57, 530–538.

67. Rückamp, D.; Martius, C.; Bragança, M.A.L.; Amelung, W. Lignin patterns in soil and termite nests of the Brazilian Cerrado. *Appl. Soil Ecol*. **2011**, 48, 45–52.
68. Hindi, S.S. Differentiation and synonyms standardization of amorphous and crystalline cellulosic products. *Nanosci. Nanotechnol. Res*. **2017a**, *4*, 73–85.
69. Hindi, S.S. Microcrystalline cellulose: The inexhaustible treasure for pharmaceutical industry. *Nanosci. Nanotechnol. Res*. **2017 b**, *4*, 22–31.
70. Hindi, S.S. Suitability of date palm leaflets for sulphated cellulose nanocrystals synthesis. *Nanosci. Nanotechnol. Res*. **2017 c**, *4*, 7–16.
71. Hindi, S.S. Nanocrystalline cellulose: Synthesis from pruning waste of *Zizyphus spina christi* and characterization. *Nanosci. Nanotechnol. Res*. **2017 d**, *4*, 106–114.
72. Hindi, S.S.; Abouhassan, R.A. Method for making nanoocrystalline cellulose. U.S. Patent No. 10,144,786B2, 4 December **2018**.
73. Hindi, S.S. A Method for converting micro- to nanocrystalline cellulose. U.S. Patent No. 10808045, 20 October **2020**.
74. Hindi, S.S. Nanocrystalline cellulose. U.S. Patent No. 11,161,918, 2 November **2021**.
75. Hindi, S.S. Urchin-shaped nanocrystalline material. U.S. Patent No. 11242410, 8 February **2022 a**.
76. Hindi, S.S. Sulfate-grafted nanocrystalline cellulose. U.S. Patent No. 11242411, 8 February **2022 b**.
77. Hindi, S.S. Evaluation of guaiacol and syringol emission upon wood pyrolysis for some fast growing species. Paper presented at the ICEBESE: International Conference on Environmental, Biological, and Ecological Sciences, and Engineering to be held during August: 24–26, **2011**, Paris, France.
78. Hindi, S.S.; Abdel-Rahman, G.M.; AL–Qubaie, A.I. Gross heat of combustion for some Saudi hardwoods. *Int. j. sci. eng. investig*. **2012 a**, 1, 10–14.
79. Hindi, S.S. Effect of maximum final temperature on properties of wood based biocarbon of *Tamarix Aphylla*. *Int. j. sci. eng. investig*. **2012 b**, ,: 1–4.
80. Hindi, S.S. Contribution of parent wood to the final properties of the carbonaceous skeleton via pyrolysis. *Int. j. sci. eng. investig*. **2012 c**, 1, 89–96.
81. Hindi, S.S. Fluids production from wood wastes via pyrolysis. *Int. j. sci. eng. investig*. **2012 d**, 1, 31–42.
82. Hindi, S.S. Effect of wood material and pyrolytic conditions on biocarbon production. *Int. J. Modern Eng. Res*. **2012 e**, 2, 1386–1394.
83. Jackson, M.L. Soil chemical analysis. Prentice-Hall, Inc. Englewood Cliffs, N. J. New Delhi, India. 1973.
84. ASTM D 2974 – Standard test methods for moisture, ash, and organic matter of peat and organic soils.
85. Hoogsteen, M.J.J.; Lantinga, E.A.; Bakker, E.J.; Groot, J.C.J.; Tittonell, P.A. Estimating soil organic carbon through loss on ignition: effects of ignition conditions and structural water loss. *Eur. J. Soil Sci*. **2015**, 66, 320–328.
86. FernandesIldeu, R.B.A.; Emerson, A.C.J.; Junior, S.R.; Mendonça, E.S. Comparison of different methods for the determination of total organic carbon and humic substances in Brazilian soils. *Nutrição de Plantas Rev. Ceres*. **2015**, 62, 496–501.
87. ASTM. D 2395-84. 1989. Standard test method for ash in wood. Philadelphia, Pa. USA.
88. ASTM. D 1105-84. 1989. Standard method for preparation of extractive-free wood. Philadelphia, Pa. USA.
89. Trilokesh, C.; Uppuluri, K.B. Isolation and characterization of cellulose nanocrystals from jackfruit peel. Sci Rep. **2019** Nov 13;9(1):16709.
90. Wise, L.E.; Merphy, M,M.D.; Adieco, M. Chlorite holocellulose, its fractionation and bearing on summative wood analysis and on studies on the hemicelluloses. *Pap. Trade J*. **1946**, 122, 35–43.
91. ASTM. D 1106–84. 1989. Standard test method for acid-insoluble lignin in wood. Philadelphia, Pa. USA.
92. Jayme, G.; Knolle, H.; Rapp, G. Development and final version of lignin determination method according to Jayme-Knolle. Das Papier. **1958**, 12 (17/18), 464–467.
93. ASTM. D 2015–85.1987. Standard test method for gross calorific value of coal and coke by the adiabatic bomb calorimeter. Philadelphia, Pa. USA.
94. Neenan, M.; Steinbeck. Calorific values for young sprouts in hardwood species. *Forest sci*. **1979**, 25, 455–461.
95. Zachariah, N.; Singh, S.; Murthy, T.; Borges, R. Bi-layered architecture facilitates high strength and ventilation in nest mounds of fungus-farming termites. *Scientific Reports*. **2020**, 10. 13157.
96. Guarino, V.; Caus, F.; Ambrosio, L. Porosity and mechanical properties relationship in PCL porous scaffolds. *J. Appl. Biomater. Biomech*. 2007 5, 149-157.
97. Hindi, S.S. Some crystallographic properties of cellulose I as affected by cellulosic resource, smoothing, and computation methods. *Int. J. Innov. Res. Technol. Sci. Eng*. **2017 e**, 6, 732–752.
98. El-Nakhlawy, F.S. Experimental design and analysis in scientific research; Sci. Pub. Center, King Abdulaziz University, Jeddah, Saudi Arabia, **2009**.
99. Korb, J., Linsenmair, K. Thermoregulation of termite mounds: what role does ambient temperature and metabolism of the colony play?. *Insectes soc*. **2000**, 47, 357–363.

100. King, H.; Ocko, S.; Mahadevan, L. Termite mounds harness diurnal temperature oscillations for ventilation. Proc. Natl. Acad. Sci. USA, **2015**, 112, 11589–11593.
101. Asiry, K.A; Nurul Huda, M.d.; Mousa, M. & Abundance and population dynamics of the key insect pests and agronomic traits of tomato (*Solanum lycopersicon* L.) varieties under different planting densities as a sustainable pest control method. *Horticulturae*. **2022**, 8. 976.
102. Wang, J.Y.; Jamil, M.; AlOtaibi, T.S.; Abdelaziz, M.E.; Ota, T.; Ibrahim, O.H.; Berqdar, L.; Asami, T.; Mousa, M.A.A.; Al-Babili, S. Zaxinone mimics (MiZax) efficiently promote growth and production of potato and strawberry Plants under Desert Climate Conditions. **2023**. 11f4c693-ac07-4c51-854d-82c41111d7c3.pdf (kaust.edu.sa) ((accessed on 11 July 2023).
103. Hindi, S.S.; Bakhashwain, A.A.; El-Feel, A.A. Physico-chemical characterization of some Saudi lignocellulosic natural resources and their suitability for fiber production. *JKAU; Met. Env. Arid Land Agric. Sci*. **2011**, 21, 45-55.
104. Hindi, S.S. 2017. Some Promising Hardwoods for Cellulose Production: I. Chemical and Anatomical Features. J. *Nanosci. Nanotechnol. Res*. **2017**, 4, 86-97.
105. Lopez, F.; Garcia, M.M.; Yanez, R.; Tapias, R.; Fernandez, M.; Diaz, M.J. Leucaena species valoration for biomass and paper production in 1 and 2 year harvest. Biores. Technol. 2008, 99, 4846-4853.
106. Diaz, M.J.; Garcia, M.M.; Eugenio, M.M.; Tapias, R.; Fernandez, M.; Lopez, F. Variations in fiber length and some pulp chemical properties of leucaena varieties. *Indust. Crops Prod*. 2007, 26, 142-150.
107. Khristova, P.; Kordsachia, O.; Khider, T. Alkaline pulping with additives of date palm rachis and leaves from Sudan. Biores. Technol. 2005, 96, 79-85.
108. Hindi, S.S. Method for recovery of cellulosic material from waste lingocellulosic material. US Patent, issue no. 11136715, issue date: 10 May **2021a**.
109. Hindi, S.S. A method for isolating alpha cellulose from lignocellulosic materials. U.S. patent, issue number 11078624, issue date: 03 August **2021b**.
110. Hindi, S.S. Method for separating lignin from lignocellulosic material. US Patent, issue no. 11, 306, 434B2, issue date: 18 April **2022**.
111. Creffield, J.W. Wood-destroying Insects–Wood borers and termites. CSIRO Publishing, Collingwood, Victoria. **1996**, 44 pp.
112. Creffield, J.W. Call for the immediate declaration of all municipalities [metropolitan Melbourne and regional Victoria] as regions where homes, buildings and structures are subject to termite infestation. **2005**, 1–21.
113. Shaikh, H.M.; Anis, A.; Poulose, A.M.; Al-Zahrani, S.M.; Madhar, N.A.; Alhamidi, A.; Alam, M.A. Isolation and characterization of alpha and nanocrystalline cellulose from date palm (*Phoenix dactylifera* L.) trunk mesh. *Polym*. **2021**, 13, 1893.
114. Liu, J.; Song, Z. ; Lu, Y. ; Wang, Q. ; Kong, F. ; Bu, F. ; Kanungo, D. ; Sun, S. Improvement effect of water-based organic polymer on the strength properties of fiber glass reinforced sand. *Polym*. **2018**, 10, 836.